




RESEARCH ARTICLE

10.1029/2021MS002539

Using Radiative Convective Equilibrium to Explore Clouds and Climate in the Community Atmosphere Model

 Kevin A. Reed¹ , Levi G. Silvers¹ , Allison A. Wing² , I-Kuan Hu³ , and Brian Medeiros⁴ 
¹School of Marine and Atmospheric Sciences, State University of New York at Stony Brook, Stony Brook, NY, USA,²Department of Earth, Ocean, and Atmospheric Science, Florida State University, Tallahassee, FL, USA, ³Rosenstiel School of Marine and Atmospheric Science, University of Miami, Miami, FL, USA, ⁴National Center for Atmospheric Research, Boulder, CO, USA**Special Section:**

Using radiative-convective equilibrium to understand convective organization, clouds, and tropical climate

Key Points:

- A new radiative-convective equilibrium (RCE) configuration is added to the official release of Community Earth System Model (CESM) to facilitate the use of Radiative-Convective Equilibrium Model Intercomparison Project (RCEMIP) in the CESM hierarchy
- The Community Atmosphere Model version 5 and Community Atmosphere Model version 6 (CAM6) RCEMIP climate states and variation across SST experiments are documented in the context of the CESM hierarchy
- Differing parameterizations lead to a reduction of low-level clouds in CAM6, consistent with differences in more realistic simulations

Supporting Information:

Supporting Information may be found in the online version of this article.

Correspondence to:K. A. Reed,
kevin.reed@stonybrook.edu**Citation:**
 Reed, K. A., Silvers, L. G., Wing, A. A., Hu, I.-K., & Medeiros, B. (2021). Using radiative convective equilibrium to explore clouds and climate in the Community Atmosphere Model. *Journal of Advances in Modeling Earth Systems*, 13, e2021MS002539. <https://doi.org/10.1029/2021MS002539>
Received 8 MAR 2021
Accepted 11 NOV 2021

© 2021 The Authors. Journal of Advances in Modeling Earth Systems published by Wiley Periodicals LLC on behalf of American Geophysical Union. This is an open access article under the terms of the [Creative Commons Attribution License](https://creativecommons.org/licenses/by/4.0/), which permits use, distribution and reproduction in any medium, provided the original work is properly cited.

Abstract Characteristics of, and fundamental differences between, the radiative-convective equilibrium (RCE) climate states following the Radiative-Convective Equilibrium Model Intercomparison Project (RCEMIP) protocols in the Community Atmosphere Model version 5 (CAM5) and version 6 (CAM6) are presented. This paper explores the characteristics of clouds, moisture, precipitation and circulation in the RCE state, as well as the tropical response to surface warming, in CAM5 and CAM6 with different parameterizations. Overall, CAM5 simulates higher precipitation rates that result in larger global average precipitation, despite lower outgoing longwave radiation compared to CAM6. Differences in the structure of clouds, particularly the amount and vertical location of cloud liquid, exist between the CAM versions and can, in part, be related to distinct representations of shallow convection and boundary layer processes. Both CAM5 and CAM6 simulate similar peaks in cloud fraction, relative humidity, and cloud ice, linked to the usage of a similar deep convection parameterization. These anvil clouds rise and decrease in extent in response to surface warming. More generally, extreme precipitation, aggregation of convection, and climate sensitivity increase with warming in both CAM5 and CAM6. This analysis provides a benchmark for future studies that explore clouds, convection, and climate in CAM with the RCEMIP protocols now available in the Community Earth System Model. These results are discussed within the context of realistic climate simulations using CAM5 and CAM6, highlighting the usefulness of a hierarchical modeling approach to understanding model and parameterization sensitivities to inform model development efforts.

Plain Language Summary Clouds, circulations and rainfall in the tropics play an important role in Earth's climate. However, global climate models differ in their representation of these features, contributing to uncertainty in future climate projections. One useful tool to better understand model differences and inform efforts to improve models is to analyze idealized configurations. We explore two different numerical representations of an idealized atmosphere relevant to tropical regions to determine the impact on the characteristics of clouds, rainfall and circulations as well as the tropical atmospheric response to warming. We show that our idealized models mirror differences in the low-cloud structure in the deep tropics of more realistic models. This work also finds similarities between the two numerical representations, such as a decrease in the spatial extent of high altitude clouds with warming. As the surface is warmed, both versions also show increases in the clustering of clouds, the likelihood of extreme precipitation rates, and an estimate of how much warming would occur in response to a doubling of carbon dioxide.

1. Introduction

In recent years there has been a renaissance in the use of reduced complexity modeling, that is, focused, efficient numerical experiments in which some aspect of the configuration is simplified, to examine specific features of interest for improved scientific understanding of processes important to the climate system (Held, 2005) and for model evaluation and development (Reed & Jablonowski, 2012). The work presented here builds on the rich history of using ocean-covered representations of Earth, so-called aquaplanet configurations, to study and model various atmospheric processes. These configurations simplify the boundary conditions of atmospheric general circulation models (GCMs; Blackburn et al., 2013; Neale & Hoskins, 2000), a central component of any climate model. Idealized aquaplanet representations of the Earth's climate system have been used frequently over the last two decades to provide process-level understanding of long-standing biases in GCMs, such as inadequate representation of cloud-topped boundary layers (Medeiros et al., 2008), the double intertropical convergence zone

bias (ITCZ; e.g., Oueslati & Bellon, 2013; Williamson & Olson, 2003), tropical variability (Leroux et al., 2016), and properties which do not converge with horizontal resolution (Herrington & Reed, 2017; O'Brien et al., 2013). The aquaplanet framework has also been used to explore the impact of warming on cloud characteristics and circulations in multiple model ensembles (Medeiros et al., 2015; Stevens & Bony, 2013), offering an alternative to its full complexity counterpart to better investigate differences among Coupled Model Intercomparison Project (CMIP) models (Eyring et al., 2016; Taylor et al., 2012). Aquaplanet frameworks have also been further idealized to explore atmospheric circulations by removing moisture and statistically representing the climate system as relaxations (Held & Suarez, 1994), or by simplifying moisture processes (Thatcher & Jablonowski, 2016) and other physical processes (Frierson et al., 2006). Aquaplanet approaches also provide a baseline from which to add additional complexity, such as modifying the lower boundary condition to include simplified representations of land to explore land-sea circulations in climate models (e.g., Voigt et al., 2016) and thus facilitate the development of a hierarchy of climate models.

While aquaplanet configurations often focus on the statistical nature of the resulting idealized climate, reduced complexity frameworks have also been developed to focus on deterministic properties in the climate system and GCMs. A particularly clear example is the baroclinic wave test of Jablonowski and Williamson (2006) which compares the evolution of an idealized balanced atmospheric state that is perturbed in a controlled manner to trigger a wave in one hemisphere. While the initial work focused on dry, aquaplanet-like GCMs, it has been extended for use in limited area models (Ullrich et al., 2015) and to include moisture (Ullrich et al., 2016). As outlined in the work of Reed and Jablonowski (2012), these deterministic frameworks have been extended to include processes in the atmosphere that are dependent on moisture feedbacks, such as tropical cyclones (Reed & Jablonowski, 2011) and thermal bubbles (Herrington & Reed, 2018). The proliferation of such frameworks offers advantages in computational cost, ease of implementation (as they are initialized from analytic initial conditions), and their ability to span a range of physical complexity (e.g., moist processes). This has led to the use of such deterministic frameworks in international intercomparisons of GCM dynamical cores that include multiple process-level tests (Ullrich et al., 2017; Zarzycki et al., 2019).

One further idealization of an aquaplanet configuration that has long been of interest to the scientific community as a framework for studying the climate system is radiative-convective equilibrium (RCE). RCE is not strictly equilibrated, but is rather a statistically stationary state of balance between radiative cooling to space and atmospheric heating from deep convection. Simulations of RCE usually do not include externally forced large-scale circulations, so the flow field is the result of the atmospheric response to radiation and convection. There is a rich history of using the RCE framework to understand the atmosphere at various spatial and temporal scales. The earliest RCE modeling studies used one-dimensional models to explore these environments (e.g., Manabe & Strickler, 1964), but as computational resources have grown, two-dimensional (e.g., Held et al., 1993) and three-dimensional (e.g., Bretherton et al., 2005; Tompkins & Craig, 1998) RCE modeling studies have become possible, enabling investigation of atmospheric circulations and their relationship to the simulated environment. More recently, additional RCE configurations have been simulated with cloud-resolving models (Cloud Resolving Models [CRMs]; e.g., Cronin & Wing, 2017; Hohenegger & Stevens, 2016; C. J. Muller & Held, 2012; Patrizio & Randall, 2019; ; Singh & O'Gorman, 2015; Wing & Emanuel, 2014) and GCMs using both global domains (e.g., Arnold & Randall, 2015; Becker et al., 2017; Bony et al., 2016; Popke et al., 2013; Reed, Medeiros, et al., 2015) and planar domains (Held et al., 2007; Silvers et al., 2016). In addition, global-scale cloud-permitting model simulations are now possible (e.g., Ohno & Satoh, 2018). One benefit of this multi-faceted research effort is a concentrated focus on the impact of moisture, clouds, and convective aggregation on climate. However, these studies have also highlighted the wide variety of parameter choices and numerical configurations with which a model can simulate RCE. A recent review of this topic is provided by Wing et al. (2017).

This recent plethora of RCE modeling frameworks led to a need within the international RCE modeling community to standardize model settings so that results across model hierarchies could be compared and investigated in a meaningful manner. A community effort established the Radiative-Convective Equilibrium Model Intercomparison Project (RCMIP; Wing et al., 2018) to provide a set of standard settings for RCE modeling studies to explore long-standing challenges, including the response of clouds, convective aggregation, and circulations to warming and their impact on climate sensitivity. Ideally a standardized experimental configuration would lead to RCE converging to a common, robust response. In reality, the initial results of RCEMIP show a wide range of atmospheric states in both GCMs and CRMs. While self-aggregation is present in nearly all of the large

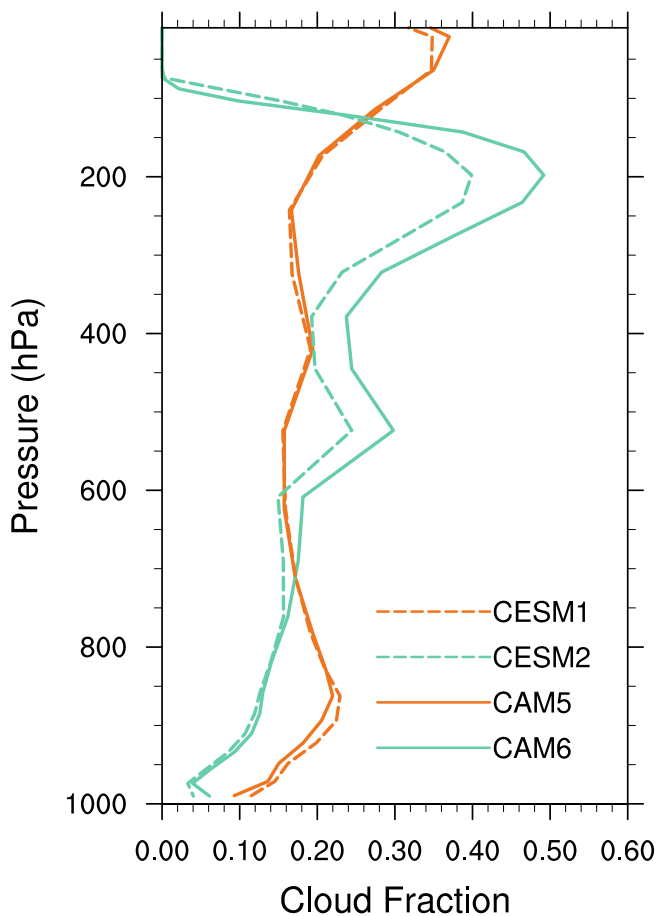


Figure 1. Average cloud fraction over the ocean covered deep tropics (5°S – 5°N) for CMIP5 (CAM5/CESM1; orange) and CMIP6 (CAM6/CESM2; green) versions of Community Earth System Model (CESM). The dashed lines represent 100 years averages from coupled Coupled Model Intercomparison Project (CMIP) CESM simulations (*piControl*) and the solid lines represent 20 years averages from the uncoupled, atmosphere-only CMIP CAM simulations (*amip*).

domain RCE simulations, Wing et al. (2020) show a lack of consensus on how self-aggregation depends on temperature. The initial results from RCE-MIP presented in Wing et al. (2020) provide an excellent starting point from which to explore the different mechanisms among the models that lead to alternate atmospheric states.

The Community Atmosphere Model (CAM) within the Community Earth System Model (CESM) provides the code-base for several models that participated in RCEMIP. CAM is unique in that it is developed by the scientific community and widely used for a variety of atmosphere- and climate-related studies. CAM offers an ability to be configured with a variety of physical parameterization suites of varying complexity which are used to investigate RCEMIP states more closely. In particular, this work will make use of CAM version 5 (CAM5 in CESM1) and the most recent version 6 (CAM6 in CESM2), which has undergone wholesale updates to the model's physical parameterizations (e.g., convection and microphysics). These modifications have led to improvements in the simulation of the Madden-Julian Oscillation, biases in low latitude shortwave cloud forcing, precipitation (Danabasoglu et al., 2020), and the large-scale circulation (Simpson et al., 2020). Despite these improvements, biases such as the double ITCZ and a climate sensitivity that is substantially larger than that of CESM1 remain (Bacmeister et al., 2020; Gettelman, Hannay, et al., 2019). In the deep tropics, the models also show large differences in tropical cloud structure, as evidenced in Figure 1. In realistic CMIP simulations CAM6 simulates more high (above 300 hPa) cloud fraction and less low (between 1,000–700 hPa) cloud fraction when compared to CAM5. RCE is thought to represent a similar tropical oceanic climate, suggesting that RCEMIP is a promising framework to explore the differences in clouds and convection in these regions, which play an important role in the Earth's climate.

The goals of this study are: (a) to provide a benchmark for future studies that use officially supported versions of CAM for RCEMIP-related analysis; (b) to investigate the relationship of precipitation, convective aggregation, circulation, and climate sensitivity to warming across two physical parameterization suites available in the official release of CAM; and (c) to set an example of the sort of targeted comparisons within the RCEMIP ensemble that can help attribute causes of the large inter-model spread. The experimental setup and the versions of CAM used in this paper are briefly described in Section 2. Section 3 provides an assessment of the RCEMIP state for CAM and investigates extreme precipitation, global energetics, aggregation, and climate sensitivity. Concluding discussions are presented in Section 4.

2. Methodology

2.1. Community Atmosphere Model

CAM is the atmospheric component of CESM developed at the National Center for Atmospheric Research (NCAR). CESM, and its predecessor the Community Climate System Model are routinely used for coupled-climate assessments (e.g., CMIP5 and CMIP6 activities; see Figure 1). For this work CAM is configured with the spectral element (SE) dynamical core option, documented most recently in Lauritzen et al. (2018). This dynamical core uses a fourth-order accurate horizontal discretization continuous Galerkin method on a cubed-sphere grid. The prognostic variables of the SE dynamical core are the two horizontal wind components, atmospheric temperature, the dry air mass, and the mass of tracers. The use of the SE dynamical core contrasts with the current CAM default finite volume dynamical core. The finite volume dynamical core, not used for this study, makes use of a regular latitude-longitude grid with large variations in horizontal grid spacing from the equator to the poles. The resulting inconsistency in horizontal scales introduce artificial inhomogeneities to RCE experiments

that make use of uniform thermodynamic forcings (see Section 2.2). The CAM SE configuration utilized in this study has a quasi-uniform 1 degree horizontal grid resolution representing a grid spacing of about 111 km, which is typical of default CESM configurations for fully coupled CMIP simulations. Note this work focuses on the versions of CAM that are part of the official publicly released version of CESM that participated in the recent RCEMIP study. Of the dozens of models that have participated in RCEMIP, CAM5 and CAM6—the focus of this work—are two out of the 11 models that completed the RCEMIP protocols on a global domain using GCM physics parameterizations. There are other CAM-based models in the RCEMIP ensemble that are not discussed here and are not part of the official NCAR CESM release.

2.1.1. CAM5

CAM5 was the default atmospheric component of the version of CESM used for CMIP5 (Taylor et al., 2012) and is the first configuration used for this work. The CAM5 physics package is documented in Neale et al. (2012). CAM5 uses the Zhang and McFarlane (1995) deep convective parameterization, which incorporates a dilute entraining plume (Neale et al., 2008), as well as convective momentum transport (Richter & Rasch, 2008). Shallow convection and moist boundary layer turbulence processes are parameterized by the University of Washington (UW) scheme (Park & Bretherton, 2009) and UW moist boundary layer turbulence scheme (Bretherton & Park, 2009), respectively. The CAM5 prognostic cloud microphysics follow the two-moment representation of cloud droplet and cloud ice of Morrison and Gettelman (2008) and the radiation scheme is the Rapid Radiative Transfer Method for GCMs (RRTMG; Iacono et al., 2008). The physics package also includes the parameterization of cloud macrophysics (Park et al., 2014), gravity wave drag, and surface fluxes as described in Neale et al. (2012).

2.1.2. CAM6

CAM6 is the most recent version of CAM in CESM that is used for CMIP6 (Eyring et al., 2016). CAM6 underwent wholesale changes from its predecessor CAM5. In particular, all boundary layer and shallow convection schemes, as well as the cloud macrophysics, are replaced by the Cloud Layers Unified by Binormals (CLUBB) parameterization. CLUBB, described in Golaz et al. (2002) and Bogenschutz et al. (2013), is a prognostic scheme for moist turbulence that uses high-order moments, closed by binormal probability density functions to describe subgrid-scale distributions of liquid water, liquid water potential temperature, total water mixing ratio, and the three velocity components. The two-moment cloud microphysics from CAM5 is also updated to include prognostic precipitation species (Gettelman & Morrison, 2015). Finally, while the Zhang and McFarlane (1995) deep convective parameterization is still used it has been substantially retuned in CAM6 compared to its predecessor, such as reducing the number of negative buoyancy regions allowed.

Considering how many elements of the CAM5 and CAM6 are different (see Table A1 for a summary of these differences), the general similarity of the atmospheric states shown in this paper is somewhat surprising. The primary common points between the models are the SE dynamical core, the radiation parameterization, surface flux representation, and components of the deep convection parameterization. Both models strive to conserve the same variables (i.e., axial angular momentum, total moist energy, total water mass, momentum, and the dry mass) but the degree to which the numerical conservation is met will be dependent on complex points of consistency between the dynamical core and the physics parameterizations (Lauritzen et al., 2018). While important, a detailed examination of the conservation properties is beyond the scope of this paper.

2.2. RCEMIP Protocols

The simulation design used here strictly follows the RCEMIP protocols described by Wing et al. (2018). In summary, homogeneous boundary conditions (i.e., following the aquaplanet configuration) are set globally by fixing the sea surface temperature (SST) to values of 295 K, 300 K, and 305 K and insolation equal to 409.6 W/m² with a solar zenith angle of 42.05°. There are no seasonal or diurnal cycles. These boundary conditions and settings ensure that every grid point receives the same insolation. Radiatively active greenhouse gases are also prescribed, as are the cloud droplet and ice crystal number concentrations ($N_c = 1.0 \times 10^8 \text{ m}^{-3}$ and $N_i = 1.0 \times 10^5 \text{ m}^{-3}$, respectively). Finally, the planetary rotation rate is set to zero. For all SST configurations the global model setup, called RCE_large, is initialized from the equilibrium profiles from the single column version of CAM (RCE_small simulations) averaged over the last 30 days of the RCEMIP 100-day simulation. Note that in the RCE_small simulations, the single column version of CAM (Gettelman, Truesdale, et al., 2019) is initialized from the RCEMIP analytic profile provided in Wing et al. (2018). This work focuses on the full 3D CAM RCE_large simulations.

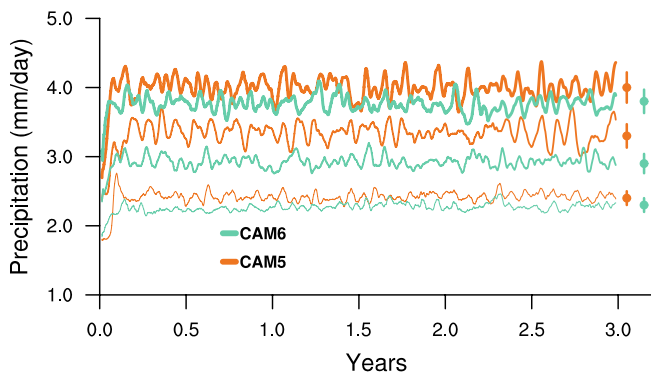


Figure 2. Domain mean precipitation time series for the radiative-convective equilibrium experiments with constant SST of 295 K, 300 K, and 305 K for CAM5 (orange) and CAM6 (green) with a 10 days running mean filter applied. Dots and lines on the right show the mean, plus and minus the standard deviation over the last year of each experiment. Thickness of the lines increases with temperature (295 K, 300 K, 305 K).

For comparison, Figure S1 in Supporting Information S1 shows profiles from the single column version of CAM and the analytical profiles from Wing et al. (2018) that have been used to initialize the RCE state. Following the RCEMIP convention the CAM simulations presented here are integrated for 3 years, though most of the analysis focuses on the last year or 100 days of output. Initially all CAM simulations experience an increase in precipitation, but an approximate steady state (which we call equilibrium) is reached within the first 75 days (Figure 2).

2.3. CAM RCEMIP Release

The RCEMIP setup in CAM is officially released as the QPRCEMIP configuration (usually called a “compset”) in the CESM2.1.2 version (publicly downloadable from: <https://github.com/ESCOMP/CESM.git>) and is available for use by the community for future RCE studies. Implementation of the QPRCEMIP compset introduced several changes to CESM2 to make the configuration more user-friendly. The rotation rate can be controlled with a runtime parameter setting. Similarly, the solar zenith angle can now be set as a uniform value with runtime parameters. An additional option was added to allow users to specify a uniform constant SST.

3. CAM RCEMIP Assessment

We provide, for future reference, an assessment of the general RCE state within CAM5 and CAM6 using the new QPRCEMIP compset. To do this we document the global energetics, the spatial structure (both horizontally and vertically), and convective aggregation. We also note the climate sensitivity that can be inferred from RCE experiments and put the values in the context of other configurations of CAM and CESM including aquaplanets and CMIP simulations. For further comparison of the climate states, mean values from the deep tropics of the parent models (from *amip* and *piControl* simulations shown in Figure 1) are tabulated. This work also represents an example of how a subset of the RCEMIP multi-model ensemble can be used for focused investigations on the response of the RCE state, precipitation, circulation and climate sensitivity to warming.

3.1. Global Energetics

Table 1 demonstrates that the global average precipitation (\bar{P}) and precipitable water (\bar{PW}) increase at different rates with warming, but to a remarkably consistent degree between the CAM5 and CAM6 RCEMIP experiments. An increase with warming of \bar{PW} is expected, theoretically, from the Clausius-Clapeyron relation and a smaller relative increase of \bar{P} is expected based on previous studies (Held & Soden, 2006; Pendergrass & Hartmann, 2014). The fractional rate of increase in \bar{PW} is approximately 13%–14% per K for both CAM RCE configurations and 6.4% per K for \bar{P} (Table 1). A stronger rate of increase in \bar{PW} relative to \bar{P} implies a slow down of the mass flux between the atmospheric boundary layer and the troposphere (Betts & Ridgway, 1988; Held & Soden, 2006). This measure of the mass flux can be approximated as \bar{P}/\bar{PW} and its decrease is nearly identical between the CAM5 and CAM6 RCE experiments.

The equilibrated \bar{P} and \bar{PW} are larger in CAM5 than CAM6 at each SST (Table 1 and Figure 2), suggesting that differences in the model physics between the CAM configurations produce systematically different RCE states. The temporal variance in the precipitation rate is also larger in CAM5 than CAM6, as can be seen in Figure 2, and this variance increases with warming in both models. It is also clear from Table 1 that less precipitation is produced from the convective parameterization in CAM6 than in CAM5. This shows that the relative role of convection and macro/microphysics parameterizations in producing precipitation in the RCEMIP simulations is different between the two CAM configurations. This is in part a result of CAM5 including the contribution from both the deep and shallow convection schemes for convective precipitation, while CAM6 only includes the contribution from deep convection.

Table 1
Comparison Between CAM5 and CAM6 RCE Simulations of Select Variables Averaged Over the Full Domain and the Last Year of the Experiment

Model	SST (K)	\bar{P} (mm/day)	\overline{PW} (kg/m ²)	\overline{CF}	\overline{OLR} (W/m ²)	\overline{ASR} (W/m ²)	\overline{LH} (W/m ²)	\overline{SH} (W/m ²)	\overline{SF}	I (hPa/day)
CAM5	295	2.43 (2.27)	23.43	0.61	239.83	319.52	70.43	11.07	0.71	126.4
	300	3.34 (2.88)	36.64	0.57	257.91	314.76	96.59	10.98	0.74	114.4
	305	3.99 (3.44)	54.65	0.51	271.52	316.30	115.5	10.10	0.74	99.3
CAM6	295	2.28 (1.69)	21.41	0.56	245.42	326.08	66.06	11.95	0.70	160.4
	300	2.93 (1.98)	31.72	0.49	260.68	326.49	84.93	12.60	0.77	156.2
	305	3.74 (2.42)	51.48	0.96	270.63	324.25	108.32	11.58	0.76	110.5

Note. Shown is the mean precipitation \bar{P} , precipitable water \overline{PW} , cloud fraction \overline{CF} , outgoing longwave radiation \overline{OLR} , the absorbed solar radiation at the top of the atmosphere \overline{ASR} , the latent \overline{LH} and sensible heat fluxes \overline{SH} , the subsidence fraction \overline{SF} , and the intensity of the large-scale circulation I. \bar{P} due to the convective parameterization is given in parenthesis. The values of I have been calculated from hourly data.

The basic energetics of CAM5 and CAM6 provide additional insight into the similarities and differences between the two models. While variations (≈ 1 W/m²) of the sensible heat flux (\overline{SH}) are expected to be small because of the prescribed SST, differences between models and experiments in the latent heat flux (\overline{LH}) are directly related to \bar{P} and are constrained to balance the net atmospheric cooling. The \overline{OLR} is strongly influenced by \overline{PW} , \overline{CF} , and the temperature of the upper-level clouds (see Section 3.2). In the 295 and 300 K experiments CAM5 has a lower average \overline{OLR} than CAM6, despite larger amounts of \bar{P} . It is unlikely that the difference in \overline{OLR} between CAM5 and CAM6 is due to differences in cloud top height, as the temperature at the upper level maximum of cloud fraction is nearly identical for the 295 and 300 K experiments (Figure 4). At 305 K, CAM5 and CAM6 have roughly the same \overline{OLR} , but \bar{P} between these experiments differs by 0.25 mm/day. This highlights how differences in the characteristics of convection or the microphysics (see Figures 3 and 4) change the degree to which the latent heating is balanced by \overline{OLR} . In particular, the larger low-level cloud fraction in CAM5 (see Figure 3) leads to additional atmospheric cooling. The influence of atmospheric cooling by low-level clouds on \bar{P} was recently discussed more thoroughly in the context of a mock-Walker circulation by Silvers and Robinson (2021). Silvers and Robinson (2021) used experiments with the longwave cloud radiative effect to show that low-level clouds are a source of atmospheric cooling because they increase the downwelling longwave radiation. Because CAM5 has more low-level clouds relative to CAM6, the additional cooling from the low-level clouds will likely contribute to more compensating \overline{LH} and \bar{P} in CAM5. CAM5 on average has a larger \overline{CF} and \overline{PW} than CAM6 (except for the anomalous case of 305 K) which is consistent with its reduced \overline{OLR} . The \overline{OLR} , \overline{PW} , and \bar{P} reach their largest values in the 305 K experiment for both models (see Section 3.3).

Mean values taken from the deep tropics of the *amip* and *piControl* experiments shown in Figure 1 are given in Table 2 and provide a picture of some similarities between the RCE configurations and the GCM parent models CAM and CESM. Analogous to the RCE experiments, CAM5 has larger \bar{P} and \overline{PW} (5.25 mm/day and 46.3 kg/m²) in the *amip* experiments relative to CAM6 (4.52 mm/day and 43.3 kg/m²). Interestingly, when the SSTs are driven by interactions between the atmosphere and ocean in the *piControl* experiments with CESM1 and CESM2 it is CESM2 which produces the most \bar{P} and \overline{PW} , rather than CESM1. We also find that for the CAM5 RCE, CAM5 GCM (*amip*), and CESM1 (*piControl*), the fraction of convective precipitation is about 90%. In contrast, the fraction of convective precipitation is about 70% in the CAM6 RCE, CAM6 GCM (*amip*), and CESM2 (*piControl*) configurations. One particular way in which the parameterization of deep convection is different between the model generations is that the number of negative buoyancy layers allowed when calculating CAPE in the scheme is reduced from five in CAM5 to one in CAM6, reducing the triggering of convection and therefore convective precipitation in CAM6. This explanation for the decrease in convective precipitation in CAM6 compared to CAM5 is consistent with the previous work by Xie et al. (2018) which showed that decreases in the number of negative buoyancy layers can suppress convection over tropical oceans in the Energy Exascale Earth System Model (which is a model sibling of CESM). The fraction of convective precipitation (often including deep and

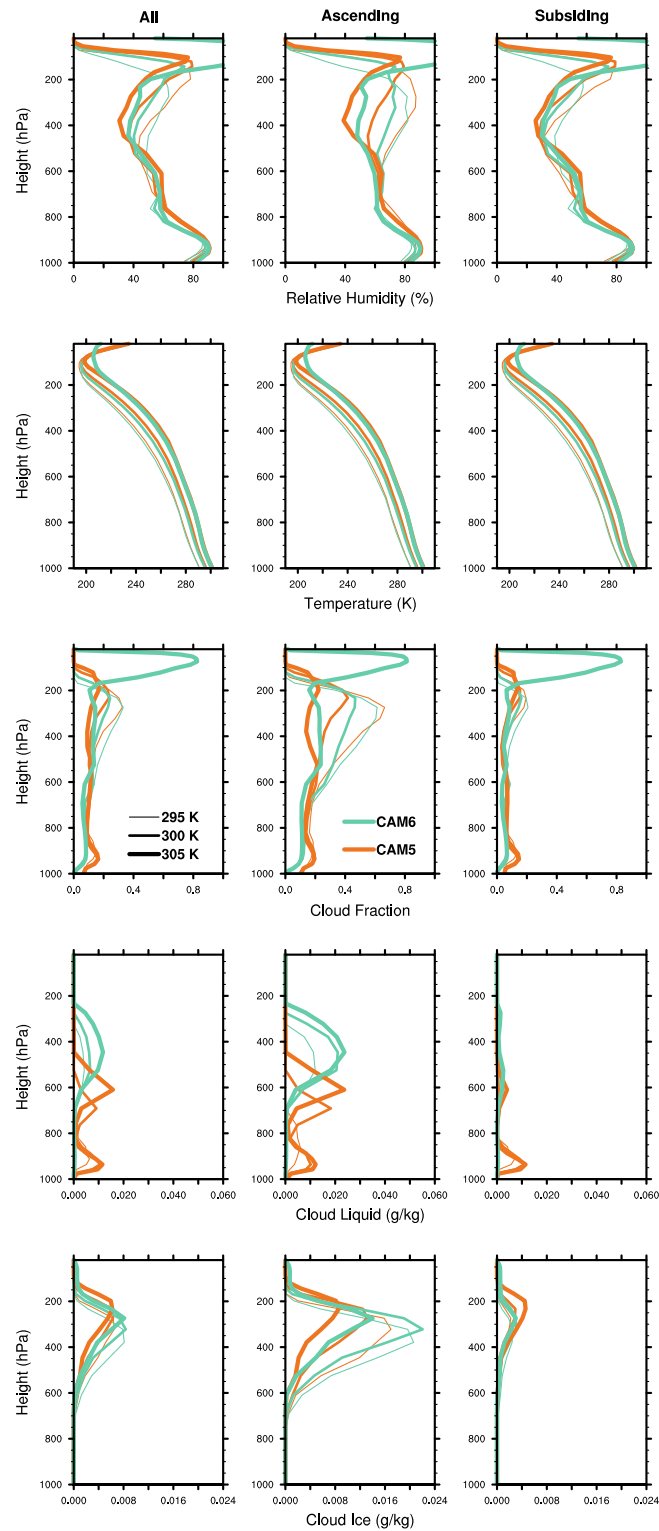


Figure 3. Globally averaged and dynamically sampled vertical profiles (as labeled, from top to bottom) of relative humidity, temperature, cloud fraction, cloud liquid, and cloud ice for the last 100 days of the Community Atmosphere Model version 5 (orange) and Community Atmosphere Model version 6 (green) RCE simulations. The hourly averaged data are separated into ascending (i.e., pressure velocity at 500 hPa less than 0.0 hPa/day) and subsiding (i.e., pressure velocity at 500 hPa greater than 0.0 hPa/day) regions in the middle and right columns. Thickness of the lines increases with temperature (295 K, 300 K, 305 K).

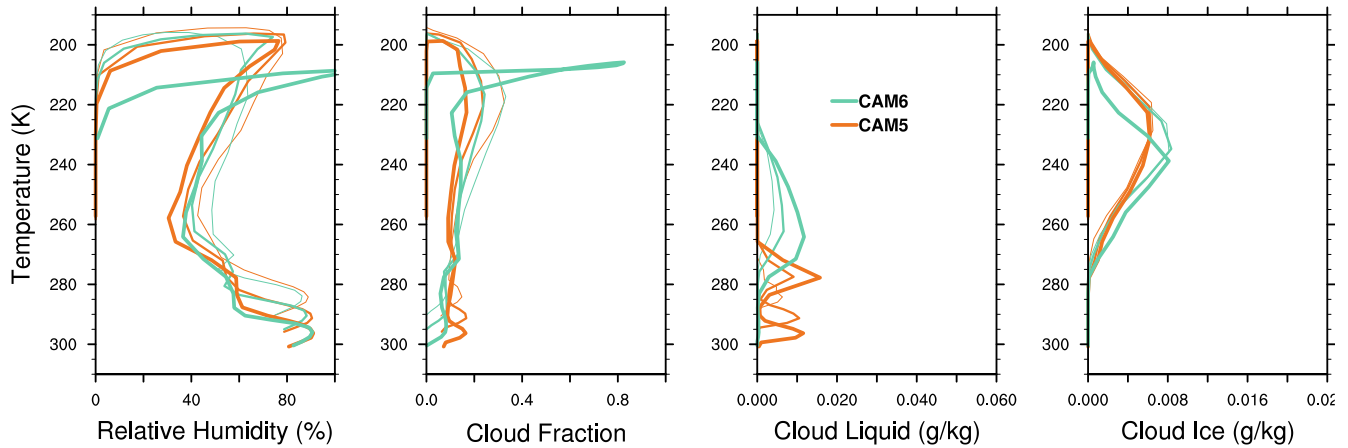


Figure 4. Globally averaged (from left to right) relative humidity cloud fraction, cloud liquid and cloud ice for the last 100 days of the Community Atmosphere Model version 5 (orange) and Community Atmosphere Model version 6 (green) RCE simulations. Thickness of the lines increases with temperature (295 K, 300 K, 305 K).

shallow convection) in a model is closely connected to basic properties of the model such as the condensate and the low cloud cover (Held et al., 2007). It is possible that some of the differences we find in \bar{P} , \overline{PW} , and cloud fraction between the fifth and sixth generation of CAM configurations could be a result of the different proportion of large-scale or convective precipitation.

To summarize, the reduction with warming of the convectively driven mass flux from the boundary layer is similar between the CAM5 and CAM6 RCE experiments. This is interesting in light of the differences in cloud liquid water, \overline{OLR} , and the fraction of convective precipitation between the two models. There are clear similarities between the RCE and *amip* configurations for each of the two model generations (CAM5 and CAM6). The CAM5 simulations tend to have more \bar{P} , \overline{PW} , \overline{LH} , and less \overline{ASR} , than CAM6. Comparisons to the parent comprehensive GCMs for mean values become more difficult when the surface is coupled to the ocean as in the *piControl* experiments. In that case it is the CESM2 model with higher amounts of \bar{P} , \overline{PW} , and \overline{ASR} .

3.2. Vertical Structure

In this section we explore the vertical structure of the RCE state between the CAM5 and CAM6 experiments. We first examine the basic thermodynamic structure and clouds of the RCE experiments. To better isolate the convective regions from the relatively cloud free regions we dynamically sample the ascending and descending regions of the domain and plot profiles from each. We then briefly discuss the response of the clouds to warming.

3.2.1. Thermodynamic State and Associated Clouds

We have shown that in the deep tropics simulated by the two generations of CAM (CAM5/CESM1 and CAM6/CESM2) in CMIP-class simulations that there are substantially more low-level clouds and less upper level clouds

Table 2
Comparison Between CAM5/CESM1 and CAM6/CESM2 of Variables (as in Table 1) Averaged Over the Ocean Covered Deep Tropics (5°S–5°N) for Official CMIP5/CMIP6 *amip* and *piControl* Experiments (Same Time Periods as in Figure 1)

Model	Simulation	\bar{P}	\overline{PW}	\overline{CF}	\overline{OLR}	\overline{ASR}	\overline{LH}	\overline{SH}
	Exp.	(mm/day)	(kg/m ²)		(W/m ²)	(W/m ²)	(W/m ²)	(W/m ²)
CESM1	<i>piControl</i>	5.06 (4.51)	42.81	0.66	251.83	306.74	113.65	12.69
CAM5	<i>amip</i>	5.25 (4.77)	46.30	0.66	248.23	304.6	112.07	12.54
CESM2	<i>piControl</i>	5.21 (3.66)	46.06	0.74	248.33	312.99	113.82	18.97
CAM6	<i>amip</i>	4.52 (3.27)	43.29	0.72	246.16	319.81	98.84	17.34

in the *amip* and *piControl* experiments of CAM5/CESM1 compared to CAM6/CESM2 (Figure 1). Investigating if these differences are also present between the CAM5 and CAM6 RCEMIP experiments would demonstrate the usefulness of the new RCEMIP compset for understanding these difference between model versions in the CESM hierarchy. Figure 3 shows vertical profiles of relative humidity, temperature, cloud fraction, cloud liquid, and cloud ice as a global average, as well as dynamically sampled into subsiding (i.e., pressure velocity at 500 hPa greater than 0.0 hPa/day) and ascending regions (i.e., pressure velocity at 500 hPa less than 0.0 hPa/day). In general, all experiments show smaller cloud fraction at all levels of the atmosphere in subsiding regions compared to ascending regions. Mid-levels in the troposphere (~800 to 200 hPa) are associated with lower relative humidity, cloud liquid, and cloud ice in the subsidence regions. Note that relative humidity, as calculated internally in CAM, is computed separately over liquid and ice when the temperature is greater than 273.15 K and less than 253.15 K, respectively, with a linear interpolation between those temperatures.

When comparing the global average cloud profile characteristics in Figure 3 there are some similarities across the experiments, particularly a peak in cloud fraction occurring above 300 hPa representing the anvils of deep convective clouds (consistent with anvil cloud heights from comprehensive simulations in Figure 1). In Figure 3 this peak in cloud fraction in the upper atmosphere is associated with a peak in relative humidity near the minimum temperature associated with the simulated tropopause. As expected, the peak cloud fraction in this upper atmosphere region is associated with a peak in the concentration of cloud ice. Lower in the atmosphere, CAM5 has a secondary peak in low level clouds in the RCEMIP simulations due to a peak in the amount of cloud liquid in the boundary layer. This peak in low-level clouds is absent from the CAM6 RCEMIP simulations.

In the context of the CESM hierarchy, analysis of Figures 1 and 3 and Table 2 reveals two types of consistency among the simulations. First, the consistency of vertical cloud structure among each configuration of a model generation (e.g., CAM5 RCEMIP, CAM5 *amip*, and CESM1 *piControl*) is seen in both CAM5/CESM1 and CAM6/CESM2. This also includes the consistency of the mean climates between the RCEMIP and *amip* simulations for each model generation (Table 1). Second, the different low-cloud structures between CESM1 and CESM2 (Figure 1) is robust across the RCE, *amip*, and *piControl* simulations. In general, consistency, as well as in the differences, in the vertical cloud structure between the two model generations are captured in the RCEMIP simulations.

It is worth noting that CAM6 is not alone in simulating few low clouds in the boundary layer under RCE conditions, as other GCMs and CRMs in the RCEMIP ensemble are shown in Wing et al. (2020) to have little or no cloud liquid and cloud fraction in this region. Exploring the differences between CAM configurations sheds light on why this might occur in CAM6. Naturally, one might expect that the CLUBB parameterization in CAM6, which replaces the boundary layer, shallow convection, and cloud macrophysics from CAM5 (see Section 2 and Table A1), is responsible for this difference in low clouds. Analysis of vertical diffusion in the CAM6 configurations indicates that the boundary layer is too diffuse and therefore cloud droplets are efficiently transported vertically, as indicated by the higher altitude of the primary peak in cloud liquid in convecting regions in CAM6 compared to CAM5 (Figure 3). To test the sensitivity of low-level cloud liquid to diffusion and evaluate it as an explanation for the difference between CAM5 and CAM6, additional sensitivity simulations with CAM6 were performed (see Figure S2 in Supporting Information S1) in which the parameter (γ) that controls the width of the vertical velocity probability density function within CLUBB is decreased from the CAM6 control value of 0.308 to 0.1, which is on the lower end of the range used in previous CLUBB parameter sensitivity studies (Guo et al., 2015; Qian et al., 2018; Zhang et al., 2018). Reducing this width parameter of the vertical velocity distribution is expected to decrease upward vertical mixing and increase lower-level clouds (Gettelman, Truesdale, et al., 2019). This result is observed in the supplemental CAM6 γ sensitivity simulations (with a smaller width parameter, γ) where the low cloud fraction and liquid increase in the boundary layer with a larger magnitude and higher altitude peak when compared to CAM5 (see Figure S2 in Supporting Information S1). It is worth mentioning, that the impact of CLUBB on the differences between CAM6 and CAM5 RCE states is likely broader than its impact on low clouds.

This demonstrates how the relative simplicity of RCE facilitates the testing of particular parameters in CAM. For such experiments RCEMIP provides important context on the idealized state while the more comprehensive CAM and CESM simulations can illustrate implications of parameter sensitivity and additional processes in the full Earth system configurations. This type of process motivated experiment could facilitate using the subset of RCEMIP large eddy simulations as a reference when examining parameterization settings (such as those in

CLUBB) for tropical convection. This may be especially valuable since CAM simulations with CLUBB have been shown to decrease low level clouds in regions of deep convection in the tropics (i.e., ITCZ and west Pacific warm pool) in more realistic simulations (e.g., Song et al., 2018), as well as in *amip* and *piControl* experiments shown in Figure 1. This example of using physical intuition, an understanding of how CAM parameterizations are designed to work, and the multi-model RCEMIP ensemble to adjust parameterizations illustrates the potential for RCE experiments to inform new GCM developments and to deepen our understanding of more realistic configurations.

3.2.2. Response of Clouds to Warming

As the SST increases, both CAM5 and CAM6 simulate little change in low level cloud fraction with warming, consistent with minimal changes of relative humidity and cloud liquid below 800 hPa (Figure 3). However, both models simulate a decrease in the anvil cloud fraction and a shift in these anvils towards lower pressures with increasing SST. There is an increase in cloud fraction above 200 hPa in the CAM6 305 K SST experiment that represents an optically thin cloud throughout most of the global domain (in both subsiding and ascending regions). As shown in Figure 3 relative humidity jumps to 100% near the tropopause in both subsiding and ascending regions in the CAM6 305 K SST experiment, which is also linked to a relatively warm tropopause temperature compared to all other experiments. It is worth noting that in more realistic simulations (Figure 1) CAM6 also simulates a higher cloud fraction (though not of the same magnitude shown in Figure 3) in these regions, compared to CAM5. Additional experiments (not shown) indicate that if the ice crystal number concentration N_i is decreased then the cloud fraction systematically decreases at these levels. One might hypothesize that the vertical mixing in CAM6, particularly in the 305 K experiment, transports cloud condensate high enough to reach the stratosphere (e.g., cloud liquid nearly reaching the 200 mb level) due to the high diffusivity of CLUBB under the RCE conditions. This leads to large amounts of supersaturation, excessive relative humidity, and too many resultant ice clouds. However, this can not be the whole story, as supplemental CAM6 gamma sensitivity simulations with decreased upward vertical mixing in CLUBB (see Figure S2 in Supporting Information S1) still experience large cloud fractions and relative humidity in the anvil cloud regions, suggesting that the interaction with the microphysics might be worth exploring. Since the focus of this work is to document and explore the CAM simulations completed as part of RCEMIP, further exploration of this response in the CAM6 305 K SST experiment is beyond the scope of this paper. This illustration highlights the usefulness of RCEMIP, not only to better understand the behavior of more realistic models, but also to identify potential artifacts and sensitivities that could manifest themselves in more Earth-like model configurations.

Excepting the outlying CAM6 305 K simulation, the anvil cloud temperature (temperature at the height of the peak high cloud fraction) changes by 15%–30% of the SST change (Figure 3). As the SST increases in CAM5 the anvil cloud temperature warms only slightly from 219.6 to 221.1K and 222.6K. The CAM6 295 and 300 K experiments also show a relatively small anvil temperature change from 217.4 to 216.6K, but in the 305 K simulation it decreases significantly to 205.6K (see Table S6 in SI of Wing et al., 2020). In the 305 K CAM6 experiment, the anvil cloud height nearly doubles compared to the 295 K experiment (see Table S7 in SI of Wing et al., 2020), in contrast to the other CAM RCE experiments where the anvil cloud height only changes by a few km.

To illustrate the temperature dependence of the anvil clouds and the relative humidity profiles, and to further explore the mean RCE states of CAM5 and CAM6, Figure 4 shows global average vertical profiles of relative humidity, cloud fraction, cloud liquid and cloud ice as a function of temperature (as opposed to pressure in Figure 3). Differences in relative humidity above the boundary layer for a given SST experiment between CAM5 and CAM6 are due to differing thermal structures with pressure. This is consistent with the work of Romps (2014) which suggests that relative humidity is an invariant function of temperature. For the CAM simulations this is confirmed by the mid-tropospheric relative humidity minimum that occurs for all six simulations near a temperature of 260K. The degree to which this invariance holds is linked to the mass exchange between convection and the environment. Recall that while the deep convection parameterization is similar for both versions of CAM, differences in this mass exchange are to be expected here given the rather large differences in parameterized convective precipitation (Table 1). These differences, in combination with changes to other parameterizations, are likely responsible for the small differences in the relative humidity profiles between CAM5 and CAM6.

When plotted as a function of temperature, the vertical profiles of cloud fraction show a remarkably consistent maximum between 215–220K for the CAM configurations (the CAM6 305 K simulation notwithstanding due to the artifact discussed). Although differences between CAM5 and CAM6 are clear for cloud liquid and cloud ice,

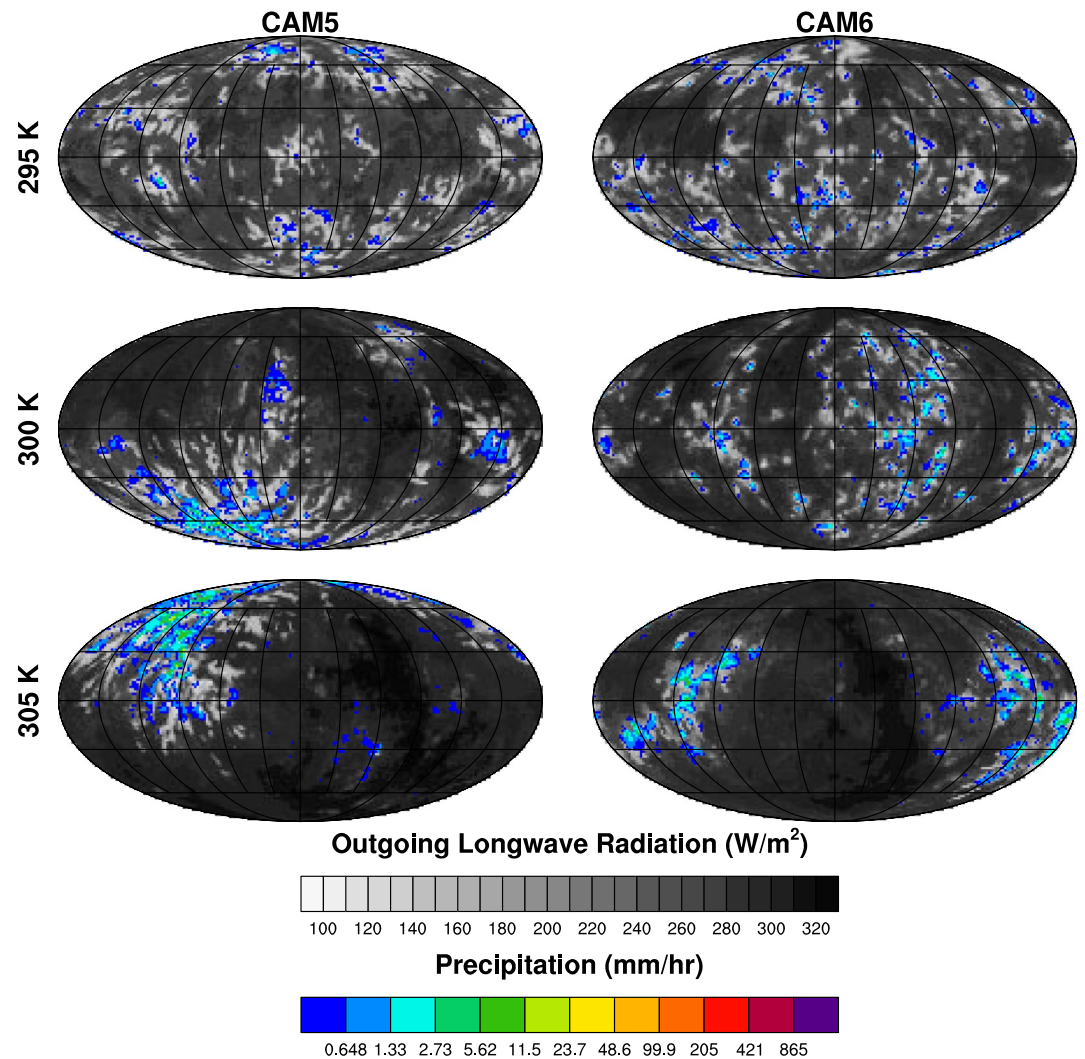


Figure 5. Hourly averaged snapshot of outgoing longwave radiation (gray shading) and total precipitation rate (color shading) from the last day of the three Community Atmosphere Model version 5 (left) and Community Atmosphere Model version 6 (right) RCE simulations with SSTs of 295 K, 300 K, and 305 K (see labels). Note, for comparison purposes the colorbars used match those in Wing et al. (2018), which introduced the RCEMIP protocols.

Figure 4 shows that each model individually is nearly temperature invariant in the upper troposphere. The distribution of total cloud condensate in CAM6 is more concentrated in the mid-troposphere relative to CAM5, with cloud liquid at colder temperatures and cloud ice at warmer temperatures. This further suggests that differences in cloud liquid and the characteristics of convection at these levels is due to wholesale differences in the shallow convection and boundary layer parameterizations between the model versions (and their interactions with the microphysics). In the free troposphere we see that for each model the relative humidity and cloud fraction are primarily functions of temperature with the maximum and minimum values being nearly invariant in temperature.

3.3. Horizontal Structure

Comparing the horizontal structures of humidity, clouds, and wind can reveal important differences between the CAM5 and CAM6 RCE states that may be missed in the global mean statistics. At a given SST, there are noticeable differences in the horizontal spatial patterns between the CAM5 and CAM6 configurations. In general, compared to CAM6, CAM5 produces more coherent clustering of convection, shown as areas of low outgoing longwave radiation and increased precipitation rates (Figure 5). This is particularly apparent at the 300 K temperature where CAM6 has more globally distributed convection than the more clustered CAM5 (Movie S1 provides

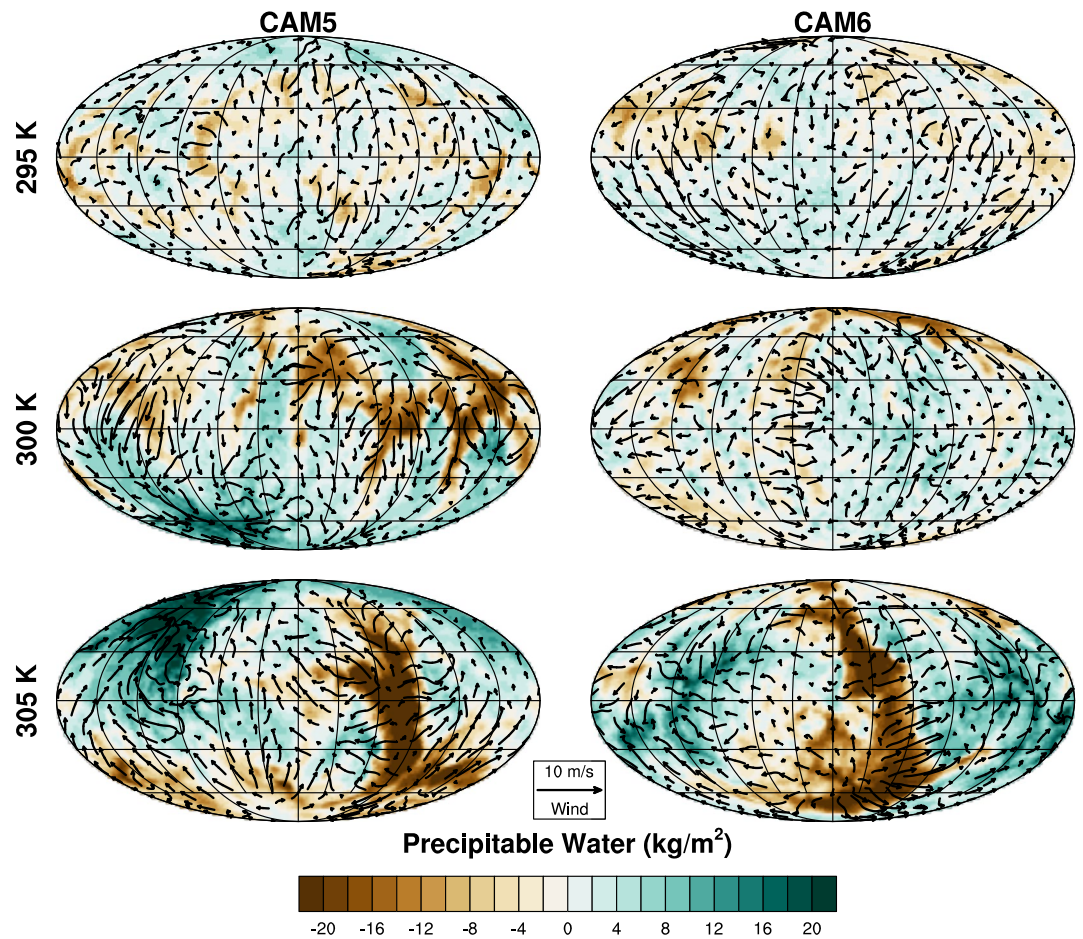


Figure 6. Hourly averaged snapshot of precipitable water anomaly (contours) and lowermost-model-level winds (vectors) from the last day of the three Community Atmosphere Model version 5 (left) and Community Atmosphere Model version 6 (right) RCE simulations with SSTs of 295 K, 300 K, and 305 K (see labels). The anomaly is calculated as the difference between the hourly averaged precipitable water and the global mean.

a look at the evolution of these fields for each CAM configuration and SST). In both CAM configurations, as the SST increases from 295 to 305 K, the convection becomes more aggregated, collapsing into one or two coherent clusters within the entire domain. This results in increased precipitation rates within the convective clusters (see Section 3.5 for scaling discussion of extreme precipitation rates). The increase in mean precipitation with warming discussed in Section 3.1 has a contribution from the changing spatial structure of convection with warming seen in Figure 5. More aggregated states have larger, drier subsidence regions (the darkest regions in Figure 5), which increases the mean atmospheric radiative cooling (and mean OLR; Table 1), thus energetically constraining mean precipitation to increase as well. As the regions of low OLR and strong precipitation become more concentrated and the dry subsiding regions expand, the mid-tropospheric RH and upper level clouds decrease, as seen in Figures 3 and 4. Note that the large upper-level cloud fraction for the CAM6 305 K experiment does not appear to influence the OLR.

Another way to view the spatial structures that are present in the RCE state is provided in Figure 6 which shows a snapshot (at the same time as Figure 5) of the precipitable water (or water vapor path) anomaly from the global mean along with the lowermost model level wind vectors. Again, it is clear that there is some difference in the RCE states between the CAM5 and CAM6 configurations at a given SST. The cloud clusters seen in Figure 5 are associated with local maxima in precipitable water while the regions of large outgoing longwave radiation values demarcate dry regions. The range of precipitable water is generally comparable between CAM5 and CAM6 at each temperature, except for the 300 K where CAM5 has more spread. As the SST increases, the range of precipitable water anomalies becomes larger. This can be associated with convective self aggregation (see Section 3.4)

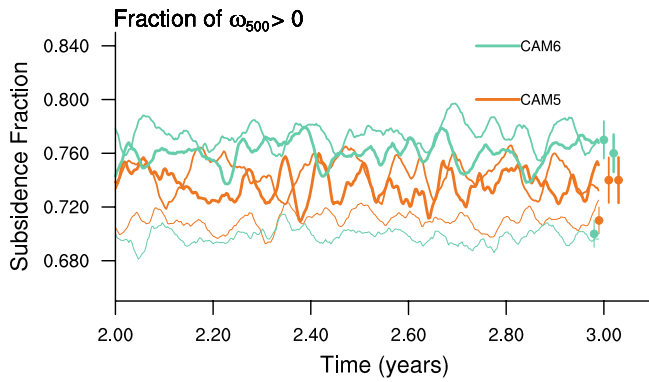


Figure 7. Subsidence fraction time series over the last year for the experiments with constant SST of 295 K, 300 K, and 305 K for Community Atmosphere Model version 5 (orange) and Community Atmosphere Model version 6 (green) RCE simulations with a 10 days running mean filter applied. Dots and lines on the right show the mean and standard deviation over the last year of each experiment. Thickness of the lines increases with temperature (295 K, 300 K, 305 K).

and increases in moisture following Clausius-Clapeyron. The wind vectors reveal a robust circulation with divergence from regions with low precipitable water and convergence into the regions with high precipitable water path, large precipitation rates and low outgoing radiation.

3.4. Convective Aggregation

As discussed in Section 3.3, the moisture, clouds and precipitation in both the CAM5 and CAM6 simulations aggregate into organized structures (Figures 5 and 6). Since this organization occurs despite homogenous initial conditions and forcing, it is referred to as convective self-aggregation. This aggregation influences the mean energetics of the simulations and appears to increase with warming in both CAM5 and CAM6, as is apparent visually (Figures 5 and 6) and as measured by the subsidence fraction (Table 1, Figure 7). The subsidence fraction (SF), which is computed on the 500 hPa level from daily averaged values of the pressure velocity field (ω_{500} ; Table 1, Figure 7), is a common metric of aggregation. After an initial adjustment of one or two months, the subsidence fraction for all experiments is steady in time (only the last year is plotted). For both CAM5 and CAM6, the SF indicates an increase in aggregation as the surface temperature rises above 295 K. Past studies have shown that SF can increase or decrease with SST, depending on the model

and the range of SST considered (e.g., an increase of SF in the GCM simulations of Coppin and Bony (2015) but a decrease in the CRM simulations of Cronin and Wing (2017)). Across RCEMIP (Wing et al., 2020), there is a large range in the values and trends of SF.

Despite the visual impression (Figures 5 and 6) of more aggregation in the CAM5 300 K experiment, the SF indicates more aggregation in CAM6 (Figure 7). Therefore, to more thoroughly compare aggregation in CAM5 and CAM6, we also consider other metrics of aggregation. The spatial variance of column relative humidity and an organization index (I_{org} ; Tompkins & Semie, 2017) have also been used as measures of aggregation and are shown across the range of RCEMIP models in Wing et al. (2020). Their Figure 12 shows that CAM5 and CAM6 have values of SF that are in the larger half of the SF range, but values of the spatial variance of column relative humidity that are on the order of 0.01; lower than most of the CRMs and GCMs. In the 300 K simulation, while SF indicates more aggregation in CAM6 than CAM5, I_{org} and the variance of column RH indicate more aggregation in CAM5 than CAM6, consistent with the appearance of Figures 5 and 6. When looking at the overall change from 295 to 305 K experiments, all three metrics show a positive change in both CAM5 and CAM6, strengthening the conclusion that aggregation increases with warming in these models (Wing et al. (2020), their Figure 16). Overall, the results from RCEMIP demonstrate that none of the three aggregation metrics (SF, I_{org} , and the variance of column RH) unambiguously identify convective self-aggregation. In particular, Wing et al. (2020) makes clear that it is challenging to identify aggregation in GCMs using I_{org} . However, with the exception of the 300 K experiment, SF and the variance of column RH agree in their comparison of CAM5 and CAM6.

To explore aggregation across the CAM reference states in more detail than can be provided by the single-valued metrics discussed above, Figure 8 shows the probability distribution of hourly average precipitable water. Consistent with Table 1 the distribution of precipitable water shifts toward higher values with increasing SST. However, Figure 8 provides more detail of how the RCE state changes with temperature. In general, as the SST increases the width of the distribution increases and becomes more negatively skewed (i.e., the dry side of the distribution has a longer tail). This increase in distribution width and skewness, which is in part due to increasing SST, indicates that both CAM5 and CAM6 become more aggregated with warming as the regions of moist convection become more concentrated and relatively drier regions more probable. This combination of changes of the distribution width and skewness also highlights some of the key differences between CAM5 and CAM6. In general, the distributions for the 295 and 305 K simulations are similar for both versions of CAM (despite CAM5 having higher values of precipitable water). This is highlighted further when the global average is removed, leaving the relative precipitable water anomaly (right side of Figure 8). In this case, the distributions are even more similar, suggesting that the simulations at these SSTs have a similar degree of organization. However, the 300 K simulations present a different story. As the CAM5 precipitable water distribution is shifted to higher values, the

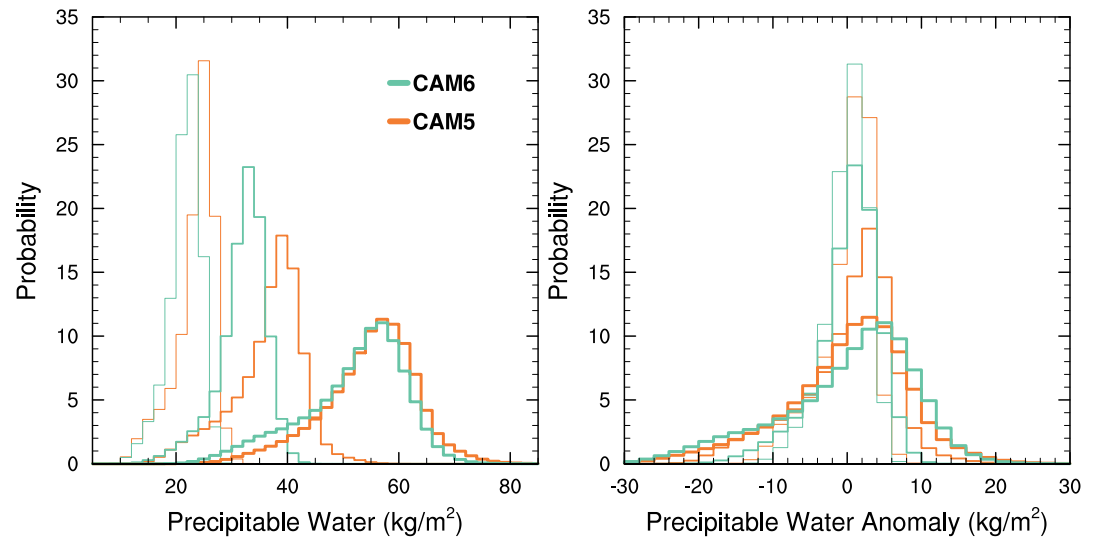


Figure 8. Probability of the 1-hourly-averaged (left) precipitable water and (right) precipitable water anomaly from the global mean for the last 100 days of each Community Atmosphere Model version 5 (orange) and Community Atmosphere Model version 6 (green) RCE simulations. The data are grouped in 2 kg/m² bins. Thickness of the lines increases with temperature (295 K, 300 K, 305 K).

anomaly distribution is wider (from -22 to 18 kg/m² in CAM5 and from -18 to 10 kg/m² in CAM6) and more negatively skewed, representing a more aggregated state in CAM5 when compared to CAM6, consistent with the visual appearance in Figures 5 and 6.

Overall, these precipitable water distributions indicate that aggregation in both versions of CAM increases with warming (in agreement with the aggregation metrics discussed above), but that CAM5 aggregates more readily with warming. This characteristic of CAM5 is not readily apparent in the subsidence fraction (Figure 7), indicating that the different metrics capture different aspects of aggregation. These precipitable water distributions also show that in general CAM5 and CAM6 are similar to each other and they both have a small range of precipitable water values relative to most other models (compare to Figure S10 from Wing et al., 2020). The similar degree of aggregation between CAM5 and CAM6 implies low sensitivity to differences in boundary layer cloud liquid. This result differs from work with CRMs in RCE (e.g., C. J. Muller & Held, 2012; C. Muller & Bony, 2015) that have shown that low clouds (and the overturning circulation induced by their radiative cooling) are essential to aggregation, which suggests that the relationship between low clouds and the degree of aggregation might be different between GCMs (shown here) and CRMs. The troposphere between 200–800 hPa is similar between CAM5 and CAM6 and we interpret this as the region of importance for aggregation. The conclusion, across all metrics considered, that both CAM5 and CAM6 show overall increased aggregation with warming is important because GCM configurations with such behavior tend to have an increased ability to cool the atmosphere. This contributes to a lower climate sensitivity relative to the RCEMIP models in which aggregation does not increase with warming (Becker & Wing, 2020; Wing et al., 2020). The climate sensitivity in the CAM models is discussed in more detail in Section 3.6.

3.5. Extreme Precipitation

While there are differences between the simulated CAM5 and CAM6 RCE states and in (*amip* and *piControl* simulations), there are some similarities in the response of the model configurations to surface warming. As shown in Section 3.1, both CAM5 and CAM6 simulate a 6.4% increase in mean total precipitation rate per K across the full 295–305 K temperature range (Table 1). The convective precipitation increases at a lower rate, 5.2% for CAM5 and 4.3% for CAM6, over the same temperature range. We assume this is due to differences in the details of the triggering of the deep convection scheme noted in Section 3.1 and results in the differences that were found between the amount of precipitation that is due to parameterized convection. This suggests that while there are differences in the global mean total and convective precipitation at a given surface temperature for CAM5 and

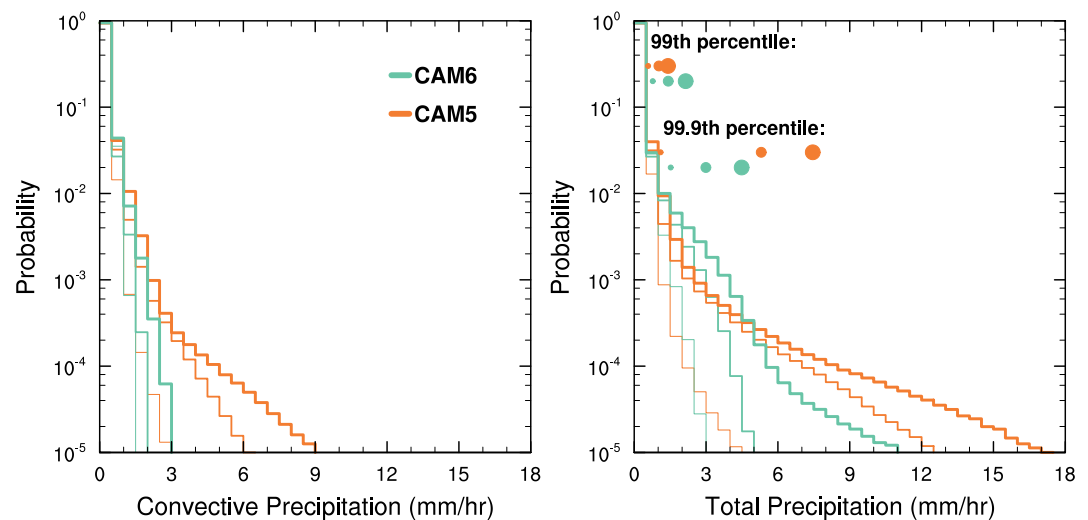


Figure 9. Probability of the 1-hourly-averaged (left) convective precipitation and (right) total precipitation for the last 100 days of each Community Atmosphere Model version 5 (orange) and Community Atmosphere Model version 6 (green) RCE simulation. The data are grouped in 0.5 mm/hr bins. For total precipitation circle markers are provided to denote the magnitude of the (top) 99 and (bottom) 99.9th percentiles. Line thickness and circle diameter increases as SST increases.

CAM6 (in RCEMIP and CMIP simulations), the simulated change with increasing SST is consistent. Figure 9 displays the probability distribution of hourly average total and convective precipitation rates for the last 100 days of each simulation to investigate the change in precipitation at different hourly rates. When focusing on extreme precipitation rates, both CAM5 and CAM6 simulate an increase in the likelihood of extreme precipitation rates with increased SST. However, that percentage change in the magnitude of the extreme precipitation with temperature increase is different between the model configurations as evident by the different shapes of the probability distributions in Figure 9. For example, CAM5 simulates a 14.4% per K increase in 99th percentile total precipitation rate from the 295–305 K experiments, while CAM6 simulates a 11.5% increase. At the 99.9th percentile total precipitation rate changes are 57.7% and 19.4% per K for CAM5 and CAM6, respectively. These large changes in the most extreme rainfall rates are consistent with previous RCE studies (Pendergrass et al., 2016) and have been shown to be linked to changes in the characteristics of the convective aggregation. The largest magnitude of change in the 99th percentile total precipitation rate occurs in the transition from 295 to 300 K in the CAM5 simulations (Figure 9), which is associated with large changes in aggregation as measured by subsidence fraction (Figure 7) and the variance in precipitable water (Figure 8). Note, that changes in the precipitation that come from the convection schemes show a similar behavior to the total precipitation across the surface temperature and model configurations, but at reduced rates in CAM6 compared to CAM5 (as discussed for mean precipitation in Section 3.1).

3.6. Climate Sensitivity

This section presents the climate sensitivity of the CAM5 and CAM6 RCE experiments and places the values in the context of several distinct model configurations which have made use of CAM (Gettelman, Hannay, et al., 2019; Gettelman et al., 2012; Medeiros et al., 2015). An integral goal of RCEMIP is to determine the dependence of climate sensitivity on both the mean cloud fields and the cloud feedbacks across the ensemble of participating models. The inferred climate sensitivity is shown in Table 3 for a range of configurations, including three iterations of CAM coupled to a slab ocean model (Gettelman, Hannay, et al., 2019) and idealized aquaplanet experiments (Medeiros et al., 2015), and the RCEMIP experiments. The inferred climate sensitivity ranges from 1.0 to 5.3K, partly as a result of the different configurations and partly because of differences among the feedback processes that are present in these models. The RCE and Aquaplanet experiments have a lower climate sensitivity than do the more Earth-like configurations. A lower climate sensitivity of RCE experiments was documented in Popke et al. (2013) and is also seen here for CAM. At least part of this is due to the absence of the positive ice-albedo feedback, but could also be due to differences of the low-clouds (i.e., the lack of stratocumulus) between the RCE configuration and those of more comprehensive configurations. The fairest comparison to the RCE climate

Table 3
Climate Sensitivities Obtained in Various Configurations of CAM and CESM

Model	Sensitivity (K)	Method	Configuration	Reference
CAM4/CCSM4	3.2	2 × CO ₂	GCM & SOM	Gettelman et al. (2012)
CAM5/CESM1	4.0	2 × CO ₂	GCM & SOM	Gettelman et al. (2012)
CAM6/CESM2	5.3	2 × CO ₂	GCM & SOM	Gettelman, Hannay, et al. (2019)
CAM4	1.7	+4K	Aquaplanet	Medeiros et al. (2015)
CAM6	2.5	+4K	Aquaplanet	Presented here
CAM5	1.0	+10K	RCEMIP	Presented here
CAM6	1.3	+10K	RCEMIP	Presented here

Note. Slab ocean models (SOM) have been used to estimate the sensitivity for CESM1 and CESM2 (Gettelman, Hannay, et al., 2019). For the Aquaplanet and RCE models, the calculation assumed a radiative forcing of 3.7 W/m². The inferred sensitivities of the RCEMIP experiments are based on the SST range of 295–305 K. The value from Medeiros et al. (2015) is based on the tropical feedback parameter.

sensitivity estimates is thus the CAM4 aquaplanet estimate from Medeiros et al. (2015), since that aquaplanet estimate was based on the tropical feedback parameter and RCE is most representative of tropical regions. Indeed, the RCE climate sensitivity is closest to, though still a bit lower than, the CAM4 aquaplanet estimate.

The climate sensitivity (CS) of particular atmospheric configurations can be inferred from constant SST perturbation experiments using the surface temperature difference (ΔT), the change in radiative flux at the top of the atmosphere (ΔR), and an assumed radiative forcing ($F_{2\times\text{CO}_2}$) that represents a CO₂ perturbation. The resulting climate feedback parameter is computed as $\lambda = \Delta R/\Delta T$ and is often referred to as the Cess feedback parameter (Cess & Potter, 1988). The inferred climate sensitivity is then given by $CS = F_{2\times\text{CO}_2}/\lambda$ (we use $F_{2\times\text{CO}_2} = 3.7 \text{ W/m}^2$ following Myhre et al., 1998). Since the actual radiative forcing in response to a doubling of CO₂ is model-dependent, this inferred climate sensitivity is not identical to the true equilibrium climate sensitivity of a given model. Nevertheless, it provides an estimate of how much warming to expect from a model that has a particular response to an imposed radiative forcing value, and allows a comparison to other warming experiments that did actually double the CO₂ concentration. For the 295/300 K experiments the CS and climate feedback values are 0.8K for CAM5 and 1.2K for CAM6. For the 300/305 K experiments the CS and climate feedback values are 1.7K for CAM5 and 1.5K for CAM6. The corresponding climate feedback parameters are $-4.7 \text{ W m}^{-2} \text{ K}^{-1}$ and $-2.5 \text{ W m}^{-2} \text{ K}^{-1}$ for CAM5 and $-3.0 \text{ W m}^{-2} \text{ K}^{-1}$ and $-2.6 \text{ W m}^{-2} \text{ K}^{-1}$ for CAM6.

The climate sensitivity shown in Table 2 increases with each of the successive generations of the CAM based models from 3.2K (CAM4) to 4.0 (CAM5/CESM1) and to 5.3K (CAM6/CESM2). The sensitivity also increased in the CAM6 Aquaplanet model relative to the CAM4 Aquaplanet. The larger sensitivity in CESM2 has been shown to be in part due to increasingly positive cloud feedbacks and the shortwave radiative feedbacks over the Southern Ocean by Gettelman, Hannay, et al. (2019) and Bacmeister et al. (2020). The inferred sensitivity of the CAM6 RCE experiment is larger than that of the CAM5 RCE experiment. The direct cause of the increased sensitivity is not due to one factor but rather a combination of changes in the shortwave, longwave, and clear sky fluxes. Despite the numerous differences in parameterization schemes there is a consistent pattern of increasing sensitivity in the successive generations of CAM. This is true for RCE, Aquaplanet, and GCM configurations. It will be important for future research to determine whether this increasing sensitivity is based on realistic physical processes or an artifact of the increasingly complex generations of CAM.

4. Conclusions and Discussion

Reference RCE simulations are presented using the CESM2.1.2 codebase for CAM versions 5 and 6 following the RCEMIP protocols with constant SSTs of 295, 300 and 305 K as outlined in Wing et al. (2018). This analysis provides a benchmark for future studies that use CAM with the released QPRCEMIP compset (in CESM2.1.2 and future releases) for RCE-related analyses that explore clouds, convection, and climate. Among the most interesting differences between the CAM5 and CAM6 RCE climates are a smaller cloud fraction in CAM6 below 500hPa and an almost complete lack of liquid water below about 700 hPa. This is consistent with the ocean covered tropical regions of the more realistic CMIP simulations (*amip* and *piControl*) in which CAM6 simulates more high

(above 300 hPa) cloud fraction and less low (between 1,000–700 hPa) cloud fraction when compared to CAM5 (Figure 1). These differences are due in part to distinct representations of shallow convection and boundary layer processes. Additionally, CAM5 RCE simulates larger precipitation rates and larger global average precipitation, despite less outgoing longwave radiation (for the 295 and 300 K experiments) compared to CAM6. Similarities in the characteristics of upper troposphere deep convective anvil clouds are observed, linked to the use of a similar deep convection parameterization. Both CAM5 and CAM6 simulate similar peaks in the height of cloud fraction, relative humidity, and cloud ice in these regions (except for the CAM6 305 K configuration due to the artifact discussed in Section 3).

When analyzed across SST experiments further similarities exist between the CAM5 and CAM6 RCEMIP experiments. The maximum upper troposphere cloud fraction decreases in magnitude and increases in height as the SST warms in both CAM5 and CAM6, consistent with previous work using RCE in GCMs (Bony et al., 2016). In general, extreme precipitation, aggregation, and climate sensitivity increase with warming to varying degrees in both the CAM5 and CAM6 RCE experiments. Over the full temperature range both CAM5 and CAM6 simulate an increase in subsidence fraction and variance in precipitable water with warming, suggesting an increase in convective aggregation. However, the rate of change in aggregation with warming depends on the model version and the choice of aggregation metric. For example, the precipitable water field suggests that relatively dry regions become more frequent as the temperature increases from 295 to 300 K in CAM5, suggesting a more aggregated state at the warmer temperature. However, for the same temperature range with CAM6 the change in the probability of relatively dry regions is less stark, despite a larger increase in the subsidence fraction between 295 and 300 K in CAM6 compared to CAM5. At 305 K both CAM5 and CAM6 produce clearly aggregated states from the precipitable water and outgoing radiation fields, despite an insignificant change in the subsidence fractions compared to the 300 K case for both model versions. This could reflect a change in the spatial scale of the aggregation. These differences in aggregation lead to differences in the distributions of precipitation and circulations. In particular, CAM5 tends to produce larger changes in extreme precipitation (defined as the 99 and 99.9 percentiles) with warming when compared to CAM6, while CAM6 simulates a larger decrease in the intensity of the circulation with warming. Finally, climate sensitivity is also shown to increase in both model versions between the lower (295–300 K) and higher (300–305 K) temperature ranges. However, there are differences in the value and rate of change of climate sensitivity between the two CAM versions, confirming that changes in the cloud structure, circulation strength, aggregation and climate sensitivity are interlinked (Becker & Wing, 2020; Wing et al., 2020).

The three SST RCEMIP experiments analyzed in this paper have been completed by dozens of models. The initial results of RCEMIP show a wide range of possible RCE climates and responses to warming (Wing et al., 2020). Among the full RCEMIP multi-model ensemble, the tropospheric temperature can vary by as much as 10K at a given level and the relative humidity can vary by a factor of 2. The height at which the convective anvil clouds occur varies by several kilometers and the maximum of low-level cloud fraction has a range from near zero to around 0.5. Across the 11 GCMs that participated in RCEMIP, the difference in anvil cloud temperature between the 295 and 305 K simulations ranges from 1.3K to 15.7K. Among these 11 GCMs, CAM5 is among those with the least variation in the anvil temperature with SST warming, and for the 295 and 300 K experiments CAM6 is also on the low end of anvil temperature variation. A preliminary analysis of how well the fixed anvil temperature and proportionately higher anvil temperature (FAT/PHAT) hypotheses hold in models of RCEMIP is given in Wing et al. (2020). Finally, it is worth noting that there was not a robust change of aggregation with warming across the full multi-model RCEMIP ensemble.

Considering the major differences in the model physics of CAM5 and CAM6, the overall similarity of many aspects of their atmospheric states in the broader context of the RCEMIP results of Wing et al. (2020) is interesting. That is, despite the differences shown, CAM5 and CAM6 are more similar to each other than they are to the rest of the RCEMIP ensemble. Both CAM5 and CAM6 show increasing aggregation with surface temperature. The profiles of temperature, relative humidity, and cloud fraction for CAM5 and CAM6 are more similar to each other than to the other models (see Figures 7b, 8, and 9 of Wing et al., 2020). In addition, the difference between CAM5 and CAM6 in the metrics used to quantify convective aggregation (subsidence fraction, organization index, and the spatial variance of column relative humidity) is only a fraction of the range among the RCEMIP multi-model ensemble. The spatial variance of column relative humidity in CAM5 and CAM6 is nearly the lowest value among the model ensemble. This seems consistent with the higher values of mid-tropospheric relative humidity and the relatively small negative clear sky feedback (Becker & Wing, 2020; Wing et al., 2020).

One possible explanation of these similarities is that the dynamical core, which is identical for both the CAM5 and CAM6 RCEMIP configurations and also sets the physics-dynamics coupling, plays an important role in establishing the RCE state through influences on circulations and advection. Previous work has demonstrated that the dynamical core of GCMs can play an important role in the characteristics of organized convection events in more realistic CAM simulations (e.g., tropical cyclones; Reed, Bameister, et al., 2015). The RCEMIP framework in CAM offers a unique framework to explore the impact of the choice of numerical scheme and physics-dynamics coupling as the number of dynamical cores with quasi-uniform grid spacing is expected to expand beyond the SE option in future releases of CESM. This will be the focus of future iterations of the Dynamical Core Model Intercomparison Project (Ullrich et al., 2017), which will include the use of the CAM RCEMIP compset documented here.

The new RCE compset for CAM within CESM, as one piece of the full RCEMIP multi-model ensemble (Wing et al., 2020), provides a powerful tool to explore convection, clouds, and circulations in a warming climate. The simplicity of RCE complements more complex model comparisons in its ability to better isolate differences among clouds and feedbacks across model versions and physics parameterizations. This study uses RCE in CAM to highlight differences in the low-level and upper level cloud fields between CAM5 and CAM6 (with implications for CMIP simulations with CESM). The RCEMIP framework provides a firm foundation from which to incrementally add complexity for exploration of the links between convection and climate. Examples include the introduction of rotation (e.g., Chavas & Reed, 2019; Merlis & Held, 2019; Wing et al., 2016), simplifying physical parameterizations (Frierson et al., 2006; Reed & Jablonowski, 2012), or using a warm patch of SST to simulate a mock-Walker circulation (Silvers & Robinson, 2021). When combined with a community modeling framework such as CESM, the standardized RCEMIP baseline offers a unique toolkit for the science community to advance our understanding of some of the most important topics in climate science and inform model development efforts.

Appendix A: Comparison of CAM5 and CAM6

Table A1 provides an overview of the differences in the parameterization components between CAM5 and CAM6. Depending on the configuration chosen, CAM5 and CAM6 could have additional aerosol-related tracers. These are neglected in RCE and therefore the prognostic variables listed, while technically incomplete for CESM1 or CESM2, are accurate for RCE with CAM5 and CAM6.

Table A1
Comparison of Select Components Between CAM5 and CAM6

Scheme/Component/Item	CESM1 (CAM5)	CESM2 (CAM6)
Dynamical Core	SE ^a used here (FV default)	Same as CAM5
Radiation	RRTMG	Same as CAM5
Turbulence	BL ^a (moist turbulence) Shallow convection ^d Grid-scale condensation ^e	CLUBB ^{b,c}
Deep Convection	Zhang-McFarlane ^f	Zhang-McFarlane ^f (minor changes)
Cloud Microphysics	MG1 ^g	MG2 ^h
Vertical Levels	30 (2.26 hPa top)	32 (2.26 hPa top)
Prognostic Variables	Zonal and meridional wind, temperature, dry air mass, water vapor, cloud liquid, cloud ice	Same as CAM5 plus rain and snow
Conserved Variables	Axial angular momentum Total moist energy Total water mass, momentum Dry mass	Same as CAM5

Note. Superscripts indicate the following citations.

^aLauritzen et al. (2018). ^bBretherton and Park (2009). ^cGolaz et al. (2002). ^dLarson (2017). ^ePark et al. (2014). ^fZhang and McFarlane (1995). ^gMorrison and Gettelman (2008). ^hGettelman and Morrison (2015).

Data Availability Statement

All official RCEMIP CAM output is publicly available at <http://hdl.handle.net/21.14101/d4bee8e-6996-453e-bbd1-ff53b6874c0e> hosted by the German Climate Computing Center (DKRZ), and native CAM output is accessible through NCAR Campaign Storage via Globus.

Acknowledgments

Reed and Silvers acknowledge support from NSF award number 1830729. Wing acknowledges support from NSF award number 1830724. Hu acknowledges support from NSF award number 1917328, and Medeiros acknowledges support from the Regional and Global Model Analysis component of the Earth and Environmental System Modeling Program of the U.S. Department of Energy via NSF IA 1844590. This material is based upon work supported by the National Center for Atmospheric Research, which is a major facility sponsored by the National Science Foundation under Cooperative Agreement No. 1852977. The authors would also like to acknowledge Dr. Colin Zarzycki (Pennsylvania State University), Dr. Vincent Larson (University of Wisconsin-Milwaukee), Dr. Andrew Gettelman (NCAR) and Dr. Adam Adam Herrington (NCAR) for guidance in exploring sensitivities in the CAM6 simulations, Gary Strand (NCAR) for help with formatting CAM output for RCEMIP, and Cheryl Craig (NCAR) for software engineering related to the QPRCEMIP compset in CESM. Finally, the authors would also like to thank four anonymous reviewers for their constructive and thorough reviews. We would like to acknowledge high-performance computing support from Cheyenne (<https://doi.org/10.5065/D6RX99HX>) provided by NCAR's Computational and Information Systems Laboratory, sponsored by the National Science Foundation.

References

- Arnold, N. P., & Randall, D. A. (2015). Global-scale convective aggregation: Implications for the Madden-Julian oscillation. *Journal of Advances in Modeling Earth Systems*, 7(4), 1499–1518. <https://doi.org/10.1002/2015MS000498>
- Bacmeister, J. T., Hannay, C., Medeiros, B., Gettelman, A., Neale, R., Fredriksen, H. B., et al. (2020). CO₂ increase experiments using the CESM: Relationship to climate sensitivity and comparison of CESM1 to CESM2. *Journal of Advances in Modeling Earth Systems*, 12(11), e2020MS002120. <https://doi.org/10.1029/2020MS002120>
- Becker, T., Stevens, B., & Hohenegger, C. (2017). Imprint of the convective parameterization and sea-surface temperature on large-scale convective self-aggregation. *Journal of Advances in Modeling Earth Systems*, 9(2), 1488–1505. <https://doi.org/10.1002/2016MS000865>
- Becker, T., & Wing, A. A. (2020). Understanding the extreme spread in climate sensitivity within the radiative-convective equilibrium model intercomparison project. *Journal of Advances in Modeling Earth Systems*, 12(10), e2020MS002165. <https://doi.org/10.1029/2020MS002165>
- Betts, A. K., & Ridgway, W. (1988). Coupling of the radiative, convective, and surface fluxes over the equatorial Pacific. *Journal of the Atmospheric Sciences*, 45(3), 522–536. [https://doi.org/10.1175/1520-0469\(1988\)045<0522:cotca>2.0.co;2](https://doi.org/10.1175/1520-0469(1988)045<0522:cotca>2.0.co;2)
- Blackburn, M., Williamson, D. L., Nakajima, K., Ohfuchi, W., Takahashi, Y. O., Hayashi, Y.-Y., et al. (2013). The aqua-planet experiment (APE): Control SST simulation. *Journal of the Meteorological Society of Japan. Ser II*, 91, 17–56. <https://doi.org/10.2151/jmsj.2013-a02>
- Bogenschutz, P. A., Gettelman, A., Morrison, H., Larson, V. E., Craig, C., & Schanen, D. P. (2013). Higher-order turbulence closure and its impact on climate simulations in the community atmosphere model. *Journal of Climate*, 26(23), 9655–9676. <https://doi.org/10.1175/JCLI-D-13-00075.1>
- Bony, S., Stevens, B., Coppin, D., Becker, T., Reed, K. A., Voigt, A., & Medeiros, B. (2016). Thermodynamic control of anvil cloud amount. *Proceedings of the National Academy of Sciences*, 113(32), 8927–8932. <https://doi.org/10.1073/pnas.1601472113>
- Bretherton, C. S., Blossey, P. N., & Khairoutdinov, M. (2005). An energy-balance analysis of deep convective self-aggregation above uniform SST. *Journal of the Atmospheric Sciences*, 62(12), 4273–4292. <https://doi.org/10.1175/JAS3614.1>
- Bretherton, C. S., & Park, S. (2009). A new moist turbulence parameterization in the Community Atmosphere Model. *Journal of Climate*, 22, 3422–3448. <https://doi.org/10.1175/2008JCLI2556.1>
- Cess, R. D., & Potter, G. L. (1988). A methodology for understanding and intercomparing atmospheric climate feedback processes in general circulation models. *Journal of Geophysical Research: Atmospheres*, 93(D7), 8305–8314. <https://doi.org/10.1029/JD093iD07p08305>
- Chavas, D. R., & Reed, K. A. (2019). Dynamical aquaplanet experiments with uniform thermal forcing: System dynamics and implications for tropical cyclone genesis and size. *Journal of the Atmospheric Sciences*, 76(8), 2257–2274. <https://doi.org/10.1175/JAS-D-19-0001.1>
- Coppin, D., & Bony, S. (2015). Physical mechanisms controlling the initiation of convective self-aggregation in a general circulation model. *Journal of Advances in Modeling Earth Systems*, 7, 2060–2078. <https://doi.org/10.1002/2015MS000571>
- Cronin, T. W., & Wing, A. A. (2017). Clouds, circulation, and climate sensitivity in a radiative-convective equilibrium channel model. *Journal of Advances in Modeling Earth Systems*, 9(8), 2883–2905. <https://doi.org/10.1002/2017MS001111>
- Danabasoglu, G., Lamarque, J.-F., Bacmeister, J., Bailey, D. A., DuVivier, A. K., Edwards, J., et al. (2020). The community earth system model version 2 (CESM2). *Journal of Advances in Modeling Earth Systems*, 12(2), e2019MS001916. <https://doi.org/10.1029/2019MS001916>
- Eyring, V., Bony, S., Meehl, G. A., Senior, C. A., Stevens, B., Stouffer, R. J., & Taylor, K. E. (2016). Overview of the Coupled Model Intercomparison Project Phase 6 (CMIP6) experimental design and organization. *Geoscientific Model Development*, 9, 1937–1958. <https://doi.org/10.5194/gmd-9-1937-2016>
- Frierson, D. M. W., Held, I. M., & Zurita-Gotor, P. (2006). A gray-radiation aquaplanet moist GCM. part I: Static stability and eddy scale. *Journal of the Atmospheric Sciences*, 63(10), 2548–2566. <https://doi.org/10.1175/JAS3753.1>
- Gettelman, A., Hannay, C., Bacmeister, J. T., Neale, R. B., Pendergrass, A. G., Danabasoglu, G., et al. (2019). High climate sensitivity in the community earth system model version 2 (CESM2). *Geophysical Research Letters*, 46(14), 8329–8337. <https://doi.org/10.1029/2019GL083978>
- Gettelman, A., Kay, J., & Shell, K. (2012). The evolution of climate sensitivity and climate feedbacks in the community atmosphere model. *Journal of Climate*, 25(5), 1453–1469. <https://doi.org/10.1175/jcli-d-11-00197.1>
- Gettelman, A., & Morrison, H. (2015). Advanced two-moment bulk microphysics for global models. Part I: Off-line tests and comparison with other schemes. *Journal of Climate*, 28(3), 1268–1287. <https://doi.org/10.1175/JCLI-D-14-00102.1>
- Gettelman, A., Truesdale, J. E., Bacmeister, J. T., Caldwell, P. M., Neale, R. B., Bogenschutz, P. A., & Simpson, I. R. (2019). The single column atmosphere model version 6 (SCAM6): Not a scam but a tool for model evaluation and development. *Journal of Advances in Modeling Earth Systems*, 11(5), 1381–1401. <https://doi.org/10.1029/2018MS001578>
- Golaz, J. C., Larson, V. E., & Cotton, W. R. (2002). A PDF-based model for boundary layer clouds. Part I: Method and model description. *Journal of the Atmospheric Sciences*, 59, 2540–2551. [https://doi.org/10.1175/1520-0469\(2002\)059<3540:apbmbf>2.0.co;2](https://doi.org/10.1175/1520-0469(2002)059<3540:apbmbf>2.0.co;2)
- Guo, Z., Wang, M., Qian, Y., Larson, V. E., Ghan, S., Ovchinnikov, M., et al. (2015). Parametric behaviors of CLUBB in simulations of low clouds in the community atmosphere model (CAM). *Journal of Advances in Modeling Earth Systems*, 7(3), 1005–1025. <https://doi.org/10.1002/2014MS000405>
- Held, I. M. (2005). The gap between simulation and understanding in climate modeling. *Bulletin of the American Meteorological Society*, 86(11), 1609–1614. <https://doi.org/10.1175/BAMS-86-11-1609>
- Held, I. M., Hemler, R. S., & Ramaswamy, V. (1993). Radiative-convective equilibrium with explicit two-dimensional moist convection. *Journal of the Atmospheric Sciences*, 50(23), 3909–3927. [https://doi.org/10.1175/1520-0469\(1993\)050<3909:rcwet>2.0.co;2](https://doi.org/10.1175/1520-0469(1993)050<3909:rcwet>2.0.co;2)
- Held, I. M., & Soden, B. J. (2006). Robust responses of the hydrological cycle to global warming. *Journal of Climate*, 19(21), 5686–5699. <https://doi.org/10.1175/JCLI3990.1>
- Held, I. M., & Suarez, M. J. (1994). A proposal for the intercomparison of the dynamical cores of atmospheric general circulation models. *Bulletin of the American Meteorological Society*, 75(10), 1825–1830. [https://doi.org/10.1175/1520-0477\(1994\)075<1825:apftio>2.0.co;2](https://doi.org/10.1175/1520-0477(1994)075<1825:apftio>2.0.co;2)
- Held, I. M., Zhao, M., & Wyman, B. (2007). Dynamic radiative-convective equilibria using GCM column physics. *Journal of the Atmospheric Sciences*, 64, 228–238. <https://doi.org/10.1175/JAS3825.11>

- Herrington, A. R., & Reed, K. A. (2017). An explanation for the sensitivity of the mean state of the community atmosphere model to horizontal resolution on aquaplanets. *Journal of Climate*, *30*(13), 4781–4797. <https://doi.org/10.1175/JCLI-D-16-0069.1>
- Herrington, A. R., & Reed, K. A. (2018). An idealized test of the response of the community atmosphere model to near-grid-scale forcing across hydrostatic resolutions. *Journal of Advances in Modeling Earth Systems*, *10*(2), 560–575. <https://doi.org/10.1002/2017MS001078>
- Hohenegger, C., & Stevens, B. (2016). Coupled radiative convective equilibrium simulations with explicit and parameterized convection. *Journal of Advances in Modeling Earth Systems*, *8*(3), 1468–1482. <https://doi.org/10.1002/2016MS000666>
- Iacono, M. J., Delamere, J. S., Mlawer, E. J., Shephard, M. W., Clough, S. A., & Collins, W. D. (2008). Radiative forcing by long-lived greenhouse gases: Calculations with the AER radiative transfer models. *Journal of Geophysical Research: Atmospheres*, *113*(D13), D13103. <https://doi.org/10.1029/2008JD009944>
- Jablonski, C., & Williamson, D. L. (2006). A baroclinic instability test case for atmospheric model dynamical cores. *Quarterly Journal of the Royal Meteorological Society: A journal of the atmospheric sciences, applied meteorology and physical oceanography*, *132*(621C), 2943–2975. <https://doi.org/10.1256/qj.06.12>
- Larson, V. E. (2017). *CLUBB-SILHS: A parameterization of subgrid variability in the atmosphere*. arXiv:1711.03675v2 [physics.ao-ph].
- Lauritzen, P. H., Nair, R. D., Herrington, A. R., Callaghan, P., Goldhaber, S., Dennis, J. M., et al. (2018). NCAR release of CAM-SE in CESM2.0: A reformulation of the spectral element dynamical core in dry-mass vertical coordinates with comprehensive treatment of condensates and energy. *Journal of Advances in Modeling Earth Systems*, *10*(7), 1537–1570. <https://doi.org/10.1029/2017MS001257>
- Leroux, S., Bellon, G., Roehrig, R., Caian, M., Klingaman, N. P., Lafore, J.-P., et al. (2016). Inter-model comparison of subseasonal tropical variability in aquaplanet experiments: Effect of a warm pool. *Journal of Advances in Modeling Earth Systems*, *8*(4), 1526–1551. <https://doi.org/10.1002/2016MS000683>
- Manabe, S., & Strickler, R. F. (1964). Thermal equilibrium of the atmosphere with a convective adjustment. *Journal of the Atmospheric Sciences*, *21*(4), 361–385. [https://doi.org/10.1175/1520-0469\(1964\)021<0361:teotaw>2.0.co;2](https://doi.org/10.1175/1520-0469(1964)021<0361:teotaw>2.0.co;2)
- Medeiros, B., Stevens, B., & Bony, S. (2015). Using aquaplanets to understand the robust responses of comprehensive climate models to forcing. *Climate Dynamics*, *44*(7), 1957–1977. <https://doi.org/10.1007/s00382-014-2138-0>
- Medeiros, B., Stevens, B., Held, I. M., Zhao, M., Williamson, D. L., Olson, J. G., & Bretherton, C. S. (2008). Aquaplanets, climate sensitivity, and low clouds. *Journal of Climate*, *21*(19), 4974–4991. <https://doi.org/10.1175/2008JCLI1995.1>
- Merlis, T. M., & Held, I. M. (2019). Aquaplanet simulations of tropical cyclones. *Current Climate Change Reports*, *5*(3), 185–195. <https://doi.org/10.1007/s40641-019-00133-y>
- Morrison, H., & Gettelman, A. (2008). A new two-moment bulk stratiform cloud microphysics scheme in the community atmosphere model, version 3 (CAM3). Part I: Description and numerical tests. *Journal of Climate*, *21*(15), 3642–3659. <https://doi.org/10.1175/2008JCLI2105.1>
- Muller, C., & Bony, S. (2015). What favors convective aggregation and why? *Geophysical Research Letters*, *42*(13), 5626–5634. <https://doi.org/10.1002/2015GL064260>
- Muller, C. J., & Held, I. M. (2012). Detailed investigation of the self-aggregation of convection in cloud-resolving simulations. *Journal of the Atmospheric Sciences*, *69*(8), 2551–2565. <https://doi.org/10.1175/JAS-D-11-0257.1>
- Myhre, G., Highwood, E. J., Shine, K. P., & Stordal, F. (1998). New estimates of radiative forcing due to well mixed greenhouse gases. *Geophysical Research Letters*, *25*(14), 2715–2718. <https://doi.org/10.1029/98GL01908>
- Neale, R. B., Chen, C. C., Gettelman, A., Lauritzen, P. H., Park, S., Williamson, D. L., & Taylor, M. A. (2012). *Description of the NCAR community atmosphere model (CAM 5.0) (NCAR tech. note nos. NCARTN-486+STR)* (p. 282.). National Center for Atmospheric Research.
- Neale, R. B., & Hoskins, B. J. (2000). A standard test for AGCMs including their physical parametrizations: I: The proposal. *Atmospheric Science Letters*, *1*, 101–107. <https://doi.org/10.1006/asle.2000.0019>
- Neale, R. B., Richter, J. H., & Jochum, M. (2008). The impact of convection on ENSO: From a delayed oscillator to a series of events. *Journal of Climate*, *21*, 5904–5924. <https://doi.org/10.1175/2008JCLI2244.1>
- O'Brien, T. A., Li, F., Collins, W. D., Rauscher, S. A., Ringler, T. D., Taylor, M., et al. (2013). Observed scaling in clouds and precipitation and scale incognizance in regional to global atmospheric models. *Journal of Climate*, *26*(23), 9313–9333. <https://doi.org/10.1175/JCLI-D-13-00005.1>
- Ohno, T., & Satoh, M. (2018). Roles of cloud microphysics on cloud responses to sea surface temperatures in radiative-convective equilibrium experiments using a high-resolution global nonhydrostatic model. *Journal of Advances in Modeling Earth Systems*, *10*(8), 1970–1989. <https://doi.org/10.1029/2018MS001386>
- Oueslati, B., & Bellon, G. (2013). Tropical precipitation regimes and mechanisms of regime transitions: Contrasting two aquaplanet general circulation models. *Climate Dynamics*, *40*(9), 2345–2358. <https://doi.org/10.1007/s00382-012-1344-x>
- Park, S., & Bretherton, C. S. (2009). The University of Washington shallow convection and moist turbulence schemes and their impact on climate simulations with the Community Atmosphere Model. *Journal of Climate*, *22*, 3449–3469. <https://doi.org/10.1175/2008JCLI2557.1>
- Park, S., Bretherton, C. S., & Rasch, P. J. (2014). Integrating cloud processes in the Community Atmosphere Model, Version 5. *Journal of Climate*, *27*, 6821–6856. <https://doi.org/10.1175/JCLI-D-14-00087.1>
- Patrizio, C. R., & Randall, D. A. (2019). Sensitivity of convective self-aggregation to domain size. *Journal of Advances in Modeling Earth Systems*, *11*(7), 1995–2019. <https://doi.org/10.1029/2019MS001672>
- Pendergrass, A. G., & Hartmann, D. L. (2014). The atmospheric energy constraint on global-mean precipitation change. *Journal of Climate*, *27*(2), 757–768. <https://doi.org/10.1175/jcli-d-13-00163.1>
- Pendergrass, A. G., Reed, K. A., & Medeiros, B. (2016). The link between extreme precipitation and convective organization in a warming climate: Global radiative-convective equilibrium simulations. *Geophysical Research Letters*, *43*(21), 11445–11452. <https://doi.org/10.1002/2016GL071285>
- Popke, D., Stevens, B., & Voigt, A. (2013). Climate and climate change in a radiative-convective equilibrium version of ECHAM6. *Journal of Advances in Modeling Earth Systems*, *5*(1), 1–14. <https://doi.org/10.1029/2012MS000191>
- Qian, Y., Wan, H., Yang, B., Golaz, J.-C., Harrop, B., Hou, Z., et al. (2018). Parametric sensitivity and uncertainty quantification in the version 1 of E3SM atmosphere model based on short perturbed parameter ensemble simulations. *Journal of Geophysical Research: Atmospheres*, *123*(23), 13046–13073. <https://doi.org/10.1029/2018JD028927>
- Reed, K. A., Bacmeister, J. T., Rosenbloom, N. A., Wehner, M. F., Bates, S. C., Lauritzen, P. H., et al. (2015). Impact of the dynamical core on the direct simulation of tropical cyclones in a high-resolution global model. *Geophysical Research Letters*, *42*(9), 3603–3608. <https://doi.org/10.1002/2015GL063974>
- Reed, K. A., & Jablonski, C. (2011). An analytic vortex initialization technique for idealized tropical cyclone studies in AGCMs. *Monthly Weather Review*, *139*(2), 689–710. <https://doi.org/10.1175/2010mwr3488.1>
- Reed, K. A., & Jablonski, C. (2012). Idealized tropical cyclone simulations of intermediate complexity: A test case for AGCMs. *Journal of Advances in Modeling Earth Systems*, *4*(2), M04001. <https://doi.org/10.1029/2011MS000099>

- Reed, K. A., Medeiros, B., Bacmeister, J. T., & Lauritzen, P. H. (2015). Global radiative–convective equilibrium in the community atmosphere model, version 5. *Journal of the Atmospheric Sciences*, 72(5), 2183–2197. <https://doi.org/10.1175/JAS-D-14-0268.1>
- Richter, J. H., & Rasch, P. J. (2008). Effects of convective momentum transport on the atmospheric circulation in the Community Atmosphere Model, version 3. *Journal of Climate*, 21, 1487–1499. <https://doi.org/10.1175/2007JCLI1789.1>
- Roms, D. M. (2014). An analytical model for tropical relative humidity. *Journal of Climate*, 27(19), 7432–7449. <https://doi.org/10.1175/jcli-d-14-00255.1>
- Silvers, L. G., & Robinson, T. (2021). Clouds and radiation in a mock-Walker circulation. *Journal of Advances in Modeling Earth Systems*, 13. <https://doi.org/10.1029/2020MS002196>
- Silvers, L. G., Stevens, B., Mauritsen, T., & Giorgetta, M. (2016). Radiative convective equilibrium as a framework for studying the interaction between convection and its large-scale environment. *Journal of Advances in Modeling Earth Systems*, 8(3), 1330–1344. <https://doi.org/10.1002/2016MS000629>
- Simpson, I. R., Bacmeister, J., Neale, R. B., Hannay, C., Gettelman, A., Garcia, R. R., et al. (2020). An evaluation of the large-scale atmospheric circulation and its variability in CESM2 and other CMIP models. *Journal of Geophysical Research: Atmospheres*, 125(13), e2020JD032835. <https://doi.org/10.1029/2020JD032835>
- Singh, M. S., & O’Gorman, P. A. (2015). Increases in moist-convective updraught velocities with warming in radiative-convective equilibrium. *Quarterly Journal of the Royal Meteorological Society*, 141(692), 2828–2838. <https://doi.org/10.1002/qj.2567>
- Song, H., Zhang, Z., Ma, P.-L., Ghan, S. J., & Wang, M. (2018). An evaluation of marine boundary layer cloud property simulations in the community atmosphere model using satellite observations: Conventional subgrid parameterization versus CLUBB. *Journal of Climate*, 31(6), 2299–2320. <https://doi.org/10.1175/JCLI-D-17-0277.1>
- Stevens, B., & Bony, S. (2013). What are climate models missing? *Science*, 340(6136), 1053–1054. <https://doi.org/10.1126/science.1237554>
- Taylor, K. E., Stouffer, R. J., & Meehl, G. A. (2012). An overview of CMIP5 and the experiment design. *Bulletin of the American Meteorological Society*, 93(4), 485–498. <https://doi.org/10.1175/bams-d-11-00094.1>
- Thatcher, D. R., & Jablonowski, C. (2016). A moist aquaplanet variant of the held–suarez test for atmospheric model dynamical cores. *Geoscientific Model Development*, 9(4), 1263–1292. <https://doi.org/10.5194/gmd-9-1263-2016>
- Tompkins, A. M., & Craig, G. C. (1998). Radiative–convective equilibrium in a three-dimensional cloud-ensemble model. *Quarterly Journal of the Royal Meteorological Society*, 124(550), 2073–2097. <https://doi.org/10.1002/qj.49712455013>
- Tompkins, A. M., & Semie, A. G. (2017). Organization of tropical convection in low vertical wind shears: Role of updraft entrainment. *Journal of Advances in Modeling Earth Systems*, 9(2), 1046–1068. <https://doi.org/10.1002/2016MS000802>
- Ullrich, P. A., Jablonowski, C., Kent, J., Lauritzen, P. H., Nair, R., Reed, K. A., et al. (2017). DCMIP2016: A review of non-hydrostatic dynamical core design and intercomparison of participating models. *Geoscientific Model Development*, 10(12), 4477–4509. <https://doi.org/10.5194/gmd-10-4477-2017>
- Ullrich, P. A., Jablonowski, C., Reed, K. A., Zarzycki, C., Lauritzen, P. H., Nair, R. D., & Verlet-Banide, A. (2016). *Dynamical core model intercomparison project (DCMIP2016) test case document*. Retrieved from <https://github.com/ClimateGlobalChange/DCMIP2016>
- Ullrich, P. A., Reed, K., & Jablonowski, C. (2015). Analytical initial conditions and an analysis of baroclinic instability waves in f-and β -plane 3D channel models. *Quarterly Journal of the Royal Meteorological Society*, 141(693), 2972–2988. <https://doi.org/10.1002/qj.2583>
- Voigt, A., Biasutti, M., Scheff, J., Bader, J., Bordoni, S., Codron, F., et al. (2016). The tropical rain belts with an annual cycle and a continent model intercomparison project: Tracmip. *Journal of Advances in Modeling Earth Systems*, 8(4), 1868–1891. <https://doi.org/10.1002/2016MS000748>
- Williamson, D. L., & Olson, J. G. (2003). Dependence of aqua-planet simulations on time step. *Quarterly Journal of the Royal Meteorological Society*, 129(591), 2049–2064. <https://doi.org/10.1256/qj.02.62>
- Wing, A. A., Camargo, S. J., & Sobel, A. H. (2016). Role of radiative–convective feedbacks in spontaneous tropical cyclogenesis in idealized numerical simulations. *Journal of the Atmospheric Sciences*, 73(7), 2633–2642. <https://doi.org/10.1175/JAS-D-15-0380.1>
- Wing, A. A., Emanuel, K., Holloway, C. E., & Muller, C. (2017). Convective self-aggregation in numerical simulations: A review. *Surveys in Geophysics*, 38(6), 1173–1197. <https://doi.org/10.1007/s10712-017-9408-4>
- Wing, A. A., & Emanuel, K. A. (2014). Physical mechanisms controlling self-aggregation of convection in idealized numerical modeling simulations. *Journal of Advances in Modeling Earth Systems*, 6(1), 59–74. <https://doi.org/10.1002/2013MS000269>
- Wing, A. A., Reed, K. A., Satoh, M., Stevens, B., Bony, S., & Ohno, T. (2018). Radiative–convective equilibrium model intercomparison project. *Geoscientific Model Development*, 11(2), 793–813. <https://doi.org/10.5194/gmd-11-793-2018>
- Wing, A. A., Stauffer, C. L., Becker, T., Reed, K. A., Ahn, M.-S., Arnold, N. P., et al. (2020). Clouds and convective self-aggregation in a multi-model ensemble of radiative-convective equilibrium simulations. *Journal of Advances in Modeling Earth Systems*, 12, e2020MS002138. <https://doi.org/10.1029/2020MS002138>
- Xie, S., Lin, W., Rasch, P. J., Ma, P.-L., Neale, R., Larson, V. E., et al. (2018). Understanding cloud and convective characteristics in version 1 of the E3SM atmosphere model. *Journal of Advances in Modeling Earth Systems*, 10(10), 2618–2644. <https://doi.org/10.1029/2018MS001350>
- Zarzycki, C. M., Jablonowski, C., Kent, J., Lauritzen, P. H., Nair, R., Reed, K. A., et al. (2019). DCMIP2016: The splitting supercell test case. *Geoscientific Model Development*, 12(3), 879–892. <https://doi.org/10.5194/gmd-12-879-2019>
- Zhang, G. J., & McFarlane, N. A. (1995). Sensitivity of climate simulations to the parameterization of cumulus convection in the Canadian Climate Centre General Circulation Model. *Atmosphere-Ocean*, 33, 407–446. <https://doi.org/10.1080/07055900.1995.9649539>
- Zhang, H., Wang, M., Guo, Z., Zhou, C., Zhou, T., Qian, Y., et al. (2018). Low-cloud feedback in CAM5-CLUBB: Physical mechanisms and parameter sensitivity analysis. *Journal of Advances in Modeling Earth Systems*, 10(11), 2844–2864. <https://doi.org/10.1029/2018MS001423>